The effect of surfactants on two-phase flows in flowlines and risers

Master thesis

E.J. Pronk

Delft University of Technology

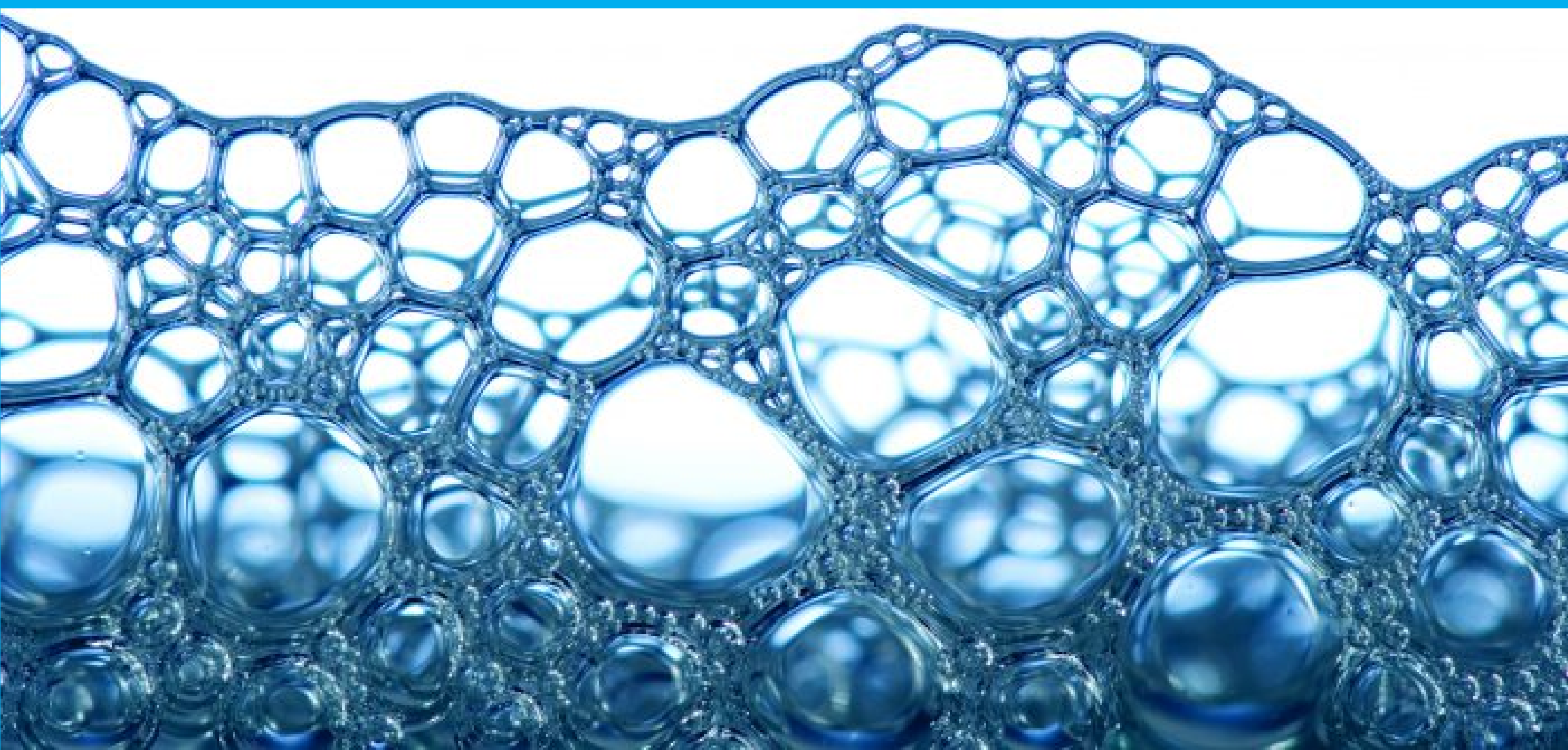

TUDelft Delft University of Technology

Challenge the future

The effect of surfactants on two-phase flows in flowlines and risers

Master thesis

by

E.J. Pronk

to obtain the degree of Master of Science in Aerospace Engineering
at the Delft University of Technology,
to be defended publicly on Friday December 15, 2017 at 10:00 AM.

Author

Name:	E.J. (Emilie) Pronk
Student number:	4094018
Project duration:	March 6, 2017 – December 15, 2017

Thesis committee

Dr. ir. B. W. van Oudheusden	TU Delft, supervisor
Prof. dr. ir. R. A. W. M. Henkes	TU Delft & Shell, supervisor
Dr. ir. M. Voskuijl	TU Delft
Dr. J. Ellepola	Shell, supervisor (guest in committee)

Faculty of Aerospace Engineering (AE) - Delft University of Technology

Preface

When I started my graduation internship in March 2017 as an aerospace engineering student, multiphase flows, slugging, surfactants and Distributed Acoustic Sensors where all new subjects to me. I got very excited and consider the opportunity to graduate at Shell as a great experience. It has not only offered me a unique experimental research, but also a way to get to know the international environment that Shell has to offer. The success of this thesis has been realized with the help of several people, who I would like to thank for their support.

First I would like to thank my three supervisors from TU Delft and Shell for supervising me the past 9 months. Jerome Ellepola was my daily Shell mentor and he was a great help during our weekly meetings. He made me realize lots of attention and follow ups are needed in order to meet deadlines when my experimental setup had to be modified. Ruud Henkes was my second Shell mentor and offered me this project, after our first chat at TU Delft. I consider him as an expert on my research topic, as he has supervised a Phd student and has (co-)written several articles in this field. His knowledge and enthusiasm for the topic where very helpful during my research. Bas van Oudheusden supervised me on behalf of the Aerodynamics Group of TU Delft. Thanks to him, I was able to write my thesis outside the faculty (or even the Flight Performance and Propulsion Group), in the inspiring environment of the Shell Technology Centre Amsterdam. Finally I would like to thank Mark Voskuijl for his time, to become part of my committee on behalf of the Flight Performance Group.

I would also like to thank Patricio Rosen for helping me with the Shell Flow Correlations, and for being a sparring partner during the final stage of my project. Murat Kerem for giving me insights into the foamer injection field trials, and good ideas with respect to the experimental matrix. As the PFAS EMEA department had no experience with the use of Distributed Acoustic Sensing, I found help at another department. I would like to thank Daria Spivakovska and Magdalena Wojtaszek for helping me out with the post-processing of the DAS data.

The Severe Slugging Loop had to be modified by the MOC team of Shell. With their work, I was able to conduct my measurements and collect the data I needed for the research. I would like to thank Jos Odijk in particular for his hands-on mentality in the MOC process.

During my internship I was assigned a coach within Shell. I would like to thank Jaap Beekers for his positivity, his advice on the experimental research and for the coaching tips regarding the Shell assessments.

Last but not least, I would like to thank my boyfriend, family and friends for their endless mental support after the Shell office hours!

Emilie J. Pronk
Delft, December 2017

Abstract

Oil and gas production systems consist of flows in wells, in horizontal and inclined flowlines and in risers. Due to the reservoir composition and changes in pressure and temperature, the flow is often under multiphase conditions. With time, the reservoir matures and the reservoir pressure decreases. The gas rate drops below a critical gas rate, that is required to produce the liquid to the wellhead and the facilities. As a result, liquids build up down-hole in the well. This phenomenon is known as liquid loading, which may kill the well. One of the deliquification methods is to use surfactants, which are injected through a capillary at the bottom of the well. Recent field trials have shown that the injection of surfactants down-hole in a well can prevent liquid loading problems. The surfactants create a foam which forms relatively thick interfacial waves along the wall of the production tubing. The gas core gets more grip on the liquid film, making it easier to produce the liquid to the surface.

Due to the success of the application of surfactants in subsurface vertical wells, it is of interest to investigate whether surfactants can also help to overcome liquid management problems in flowline-riser systems on the surface. The objective of this work is therefore to find the effect of surfactants on two-phase (air-water) flows in flowlines and risers. Experiments were carried out in the Severe Slugging Loop at the Shell Research and Technology Centre Amsterdam. The flow loop consists of a 100 m horizontal and downward inclined flowline with an inner diameter of 0.051 m, followed by a 16.8 m riser with an inner diameter of 0.044 m. The working fluids are air and water, and operation is at atmospheric outlet pressure. Two configurations of the SSL were used. In configuration #1, both water and air are injected into the flowline. The mixture is transported through the flowline to the riser. In configuration #2, water is injected into the flowline. Air is injected directly into the riser base. The dish washing detergent Dreft™ is used as a surfactant to create foam. The concentration was systematically increased to find the effect on different types of slugging (in the flowline, in the riser and severe slugging at the riser base), the pressure gradient in the riser, the developing length in the riser and the liquid and foam holdup in the riser. Various measurement techniques were used: Differential Pressure Indicators (DPIs), Pressure Indicators (PIs), Distributed Acoustic Sensors (DAS), quick closing valves and flow visualization.

When operating the SSL in configuration #1 with a superficial gas and liquid velocity of u_{SG}= 1.21 m/s and u_{SL}= 0.4 m/s, slugging in the flowline is observed. The slugs are identified as growing slugs: the stratified flow builds up regularly due to a growing instability, forming a slug. The average length of the liquid body of the slug is 32 m, the average passing time of the liquid body of the slug is 51 s, and the average slug velocity is 0.66 m/s. Through DAS and pressure measurements one can see that the slugs are mitigated when the surfactant is added. The slugs completely disappear when an effective surfactant concentration of 1000 ppm is added to the air-water mixture.

When operating the SSL in configuration #1 with a superficial gas and liquid velocity of u_{SG}= 1.4 m/s and u_{SL}= 0.27 m/s, a severe slugging cycle is found. Without surfactants, the cycle has a period of 109 s in which the riser is filled entirely with the liquid body of the slug before is is pushed out by the air. Pressure drop measurements over the riser show that adding surfactants does not prevent the slugging cycle to occur. However, the creation of foam does increase the amount of gas in the riser, making the pressure build-ups more irregular. The slugging cycle reduces to 89 s when an effective surfactant concentration of 3000 ppm is added to the air-water mixture.

When operating the SSL in configuration #2 with a superficial gas and liquid velocity of u_{SG}= 0.37 m/s and u_{SL}= 0.27 m/s, slugging in the riser is observed. Differential pressure measurements were taken over a distance of 3 m at multiple locations: one at the riser base, and two at the top of the riser. The surfactant reduces the differential pressure along the riser. For a concentration of 3000 ppm, the differential pressure reduces by 5.1% at the riser base and by 18.9% at the top of the riser.

The pressure drop curve is used to analyze the flow behaviour for a range of superficial velocities. Two types of pressure drop curves were considered: 1) for a constant superficial liquid velocity (u_{SL}= 0.05 m/s), and 2) for constant gas-to-liquid ratio (GLR= 60 and GLR= 100). For the low gas flow rate region, i.e. the gravity dominated part of the curve, both methods show a decrease in pressure gradient for a surfactant concentration of 500 ppm or greater. In the high gas flow rate region, i.e. the friction dominated part of the curve, an increase in the effective concentration leads to an increase in the pressure gradient.

The developing length of the air-water mixture with and without surfactants is analyzed by means of differential pressure measurements. Measurements were taken over a distance of 3 m at multiple locations: one at the riser base, and two at the top of the riser. With an effective concentration of 3000 ppm, the differential pressure is slightly different for the two locations on top of the riser. This indicates that the flow is not fully developed at the top of the riser. The developing length is slightly increased with the addition of the surfactant.

The foam holdup is analyzed by measuring the height of the foam between two simultaneously closed quick closing valves on the riser. The experimental results are compared with the simulation results from the Shell Flow Correlations. The experimental results show a spread due to the transient behavior of the flow. Despite the spread, the experimental results follow the trend of the simulations. At low gas flow rates, surfactants decrease the foam holdup. At high gas flow rates, surfactants increase the foam holdup. However, the foam holdup decreases for increasing gas flow rates and eventually levels off to a constant holdup value.

It can be concluded from the small-scale experiments that surfactants: 1) mitigate (growing) slugs in flowlines, 2) do not remove the severe slugging cycle, 3) decrease the pressure gradient in the riser for small gas flow rates, 4) slightly increase the development length of the flow in the riser, and 5) decrease the foam holdup for low gas flow rates, and increase the foam holdup for high gas flow rates in the riser. It is recommended to carry out the experiments on a larger scale, i.e. at higher temperatures, for larger pipe diameters, to better relate to existing flowline-riser production systems. It is also recommended to perform similar experiments to find the effect of the surfactant on other slug types, such as terrain slugs and hydrodynamic slugs, in the flowline.

List of Figures

List of Tables

Nomenclature

Abbreviations

cmc	Critical micelle concentration
DAS	Distributed Acoustic Sensing
FBE	Frequency Band Extracted
FFT	Fast Fourier Transform
GLR	Gas-to-liquid ratio
ID	Inner diameter
IPR	Inflow Performance Relationship
LGR	Liquid-to-gas ratio
SFC	Shell Flow Correlations
SFE	Shell Flow Explorer
SSL	Severe Slugging Loop
STCA	Shell Technology Centre Amsterdam
TPC	Tubing Performance Curve

Greek symbols

α	Hold-up fraction[-]
δt	Pulse duration [ns]
δz	Spatial resolution
δ	Film thickness [mm]
δ_t	Severe slugging cycle time [s]
λ	Volume fraction [-]
μ_{hb}	Bingham viscosity [$N \cdot s/m^2$]
ρ	Density [$\mathrm{kg/m^3}$]
σ	Surface tension [N/m]
τ	Wall friction or interfacial friction [$\mathrm{N/m^2}$]
φ	Pipe inclination with respect to the horizontal [°]
$\widetilde{\mu_G}$	Dimensionless gas viscosity [-]
$\widetilde{\rho_G}$	Dimensionless gas density [-]

Other symbols

$\dot{m}$	Mass fow rate [kg/s]

$\dot{q}$	Internal heat source
Π_{ss}	Severe slugging number [-]
A	Cross sectional area [m^2]
C	Surfactant concentration [ppm]
c	Speed of light [m/s]
c_p	Heat capacity [kg $\cdot$m^2/K^1$\cdot$s^2]
C_{eff}	Effective surfactant concentration [ppm]
D	Pipe diameter [m]
Eu	Euler number [-]
F	Body force [N]
f_s	Surfactant scaling factor [$-$]
Fr	Froude number [-]
g	Gravitational acceleration [m/s^2]
h	Enthalpy [J]
L	Characteristic length [m]
L_l	Length of liquid slug [m]
L_R	Length of riser [m]
n	Refractive index of fiber [-]
n	Shear index [-]
P	Pressure [N/m^2]
Q	Volumetric flow rate [m^3/s]
Re	Reynolds number [-]
S	Wetted wall perimeter [m^2]
t	Time [s]
U	Characteristic speed [m/s]
u	Averaged fluid velocity [m/s]
u_G	Actual gas velocity [m/s]
u_L	Actual liquid velocity [m/s]
u_m	Mixture velocity [m/s]
u_{SG}	Superficial gas velocity [m/s]
u_{SL}	Superficial liquid velocity [m/s]
v	Speed at which laser light propogates [m/s]
We	Weber number [$-$]
x	Streamwise coordinate [m]
z	Depth along a fiber [m]

Contents

Chapter 1

Introduction

1.1. Background

In the production of oil and natural gas, the fluids need to be transported from the reservoir to the wellhead and the facilities, where they will be processed. A schematic of a sub-sea production system is shown in Fig. 1.1. Due to the reservoir composition and changes in pressure and temperature, the flow is often under multiphase conditions; gas with condensate and water, or oil with associated gas and water. With time, the well matures and the reservoir pressure decreases. The gas rate drops below the critical gas rate, that is required to produce the liquid to the wellhead and the facilities. As a result, liquids build up down-hole, causing the well to operate under unstable flow conditions with the appearance of liquid slugs. Slugging is an irregular flow in which large pressure and flow rate fluctuations occur. The pressure on the wellhead increases and the production rate of the well declines. This phenomenon is known as liquid loading, which may kill the well. With reservoir depletion, all gas wells producing liquids will experience liquid loading. It can be recognized by an erratic decline in the production curve [8].

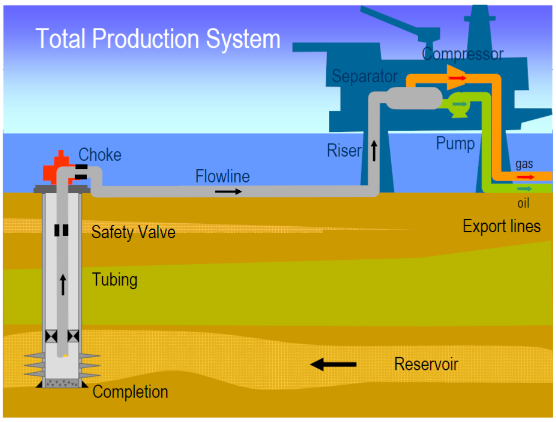

Figure 1.1: Representation of a sub-sea production system [22]

A production system can be divided into two subsystems, in order to evaluate the performance of a well. The first subsystem considers the gas flow through the reservoir towards the bottom of the well. The gas flows from the high pressured reservoir towards the bottom hole. The production rate can be shown by the reservoir Inflow Performance Relationship (IPR) curve, such as in Fig. 1.2. It shows that the reservoir pressure decreases over time (medium/low pressure curve), and that the production continues at lower gas rates.
The second subsystem considers the gas flow from the bottom-hole to the surface well head. It is depicted by the Tubing Performance Curve (TPC), also shown in Fig. 1.2. It shows the relation between the total pressure drop in the tubing, at a fixed wellhead pressure. The tubing pressure drop consists of the hydrostatic pressure loss and the frictional pressure loss. A larger liquid holdup in the tubing gives a larger value of the hydrostatic pressure loss term. The TPC passes through a minimum which divides the curve into two regions. The left part comprises the unstable, gravity dominated operating region, where liquid loading (and slugging) occurs. The right side of the TPC minimum is the stable, friction dominated operating region. This corresponds to the higher gas flow rates and bottom hole pressures.

Various deliquification techniques have been developed, in order to extend the end of field life of the reservoir production. One method is to insert a velocity string in the well. The small-diameter tubing in-

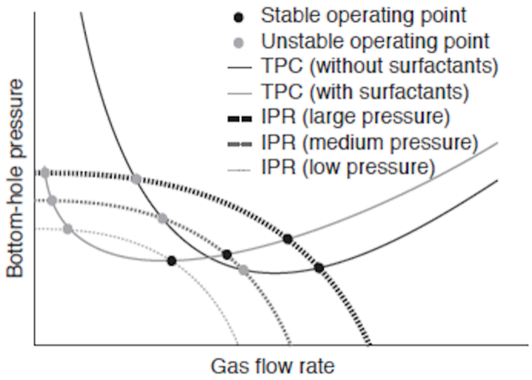

Figure 1.2: Schematic of TPC curve and IPR for gas-liquid flows. Vertical and upward inclined flows (>20 degrees from horizontal) without surfactants are shown on the left. Vertical flows with and without surfactants are shown on the right [3]

.

creases the flow velocity in the production tubing of the well, to transport the liquids to the wellhead . Another deliquification method is to use surfactants, which are injected through a capillary at the bottom of the well. It has been shown that surfactants change the TPC curve. The created foam decreases the density of the mixture compared to the liquid trapped in the well. The layer of foam forms large waves at the interface with the gas core, increasing the interfacial friction between the gas core and the liquid annulus. The gas core (which does not contain any foam, Fig. 3.5) gets more grip on the liquid film, making it easier to produce the liquid to the surface [1]. Fig. 1.2 shows the TPC curve with and without surfactants. The TPC minimum shifts to the left giving lower gas flow rates and slightly higher bottom hole pressures, thereby creating a larger stable region, i.e. multiple stable operation points. With the injection of surfactants, a well experiencing liquid loading problems can be operated again and the production of oil and gas is continued.

The use of surfactants for the deliquification of wells with relatively high gas volume fractions is a proven technology [17]. Recent foam assisted gas lift trials on an oil well in Rotterdam, the Netherlands, have shown that the injection of surfactants can increase the production by approximately 106% [10]. This outcome exceeded the production gain expectations by 20%. Furthermore, lift-gas savings of 35% could be made. The quantity of lift-gas depends on the desired gross liquid production, so even larger savings are possible.

Production systems consist of flows in wells, in horizontal and inclined flowlines and in risers, as shown in Fig. 1.1. Field trials have shown the effect of surfactants against liquid loading in wells. Van Nimwegen (2015) has studied the effect of surfactants in risers [1]. However, the effect of surfactants on flows in horizontal flowlines (with slugging) is not known. The effect of surfactants on horizontal and vertical flows has therefore been investigated in the present study. This is done through conducting experiments on an air-water mixture in a flow loop. There is in particular a large interest to assess to what extent foam-creating surfactants can mitigate or fully remove slugs in flowline-riser systems.

1.2. Research objectives

The research objective of this MSc project is:

"To improve the physical understanding of the effect of surfactants (with foam generation) on slugs in air-water horizontal and vertical pipe flows, through conducting experiments on a flow loop in which the concentration of a foaming agent is systematically is increased."

The experiments are conducted in the Severe Slugging Loop (SSL) of the Shell Research and Technology Centre in Amsterdam. The SSL is an air-water flow loop with a 100 [m] flowline followed by a 16.85 [m] vertical riser. The loop operates at atmospheric pressure and ambient temperature. Two configurations of the SSL were used (Sec. 4.1). In configuration #1, both water and air are injected into the flowline. The mixture is transported through the flowline to the riser. In configuration #2, water is injected into the flowline. Air is injected directly into the riser.

The research tasks are defined as follows:

1. Carry out experiments in the SSL in configuration #1, to find the effect of surfactants on:
   a) slugging in the flowline
   b) severe slugging at the riser base
   c) the pressure gradient

2. Carry out experiments in the SSL in configuration #2, to find the effect of surfactants on:
   a) slugging in the riser
   b) the pressure gradient
   c) the development length
   d) the holdup fraction

3. Find a relation between the concentration of the surfactant and flow stabilization

4. For vertical flows, validate the holdup experimental results with simulation results, using the Shell Flow Correlations

1.3. Literature review

In the past few years, some limited research has been done by various research teams in air-water flow loops with surfactants. The experiments distinguish themselves from others by certain parameters, such as type of surfactant, surfactant concentration, pipe diameter, pipe inclinations, and flow regimes (superficial velocities).

Christiansen (2006) [19] used a 12.2 m high vertical pipe with a diameter of 50.1 mm. As surfactant, Chapion foamatron VDF-127 was used in a 0.05 % concentration with water. An operating blower was used to introduce air into the system. The power required for this blower did not change after surfactants were added to the air-water flow with a constant gas flow rate. This is in contrast with earlier findings, where gas flow rates were reduced when surfactants were added. Also, the obtained pressure measurements did not show a significant influence of the surfactant in the flow loop. However, only a limited range of values for the superficial gas velocity was used. Furthermore, there were no visualization techniques used, nor has the influence of the concentration been researched.

Duangprasert et al. (2008) [23] used three SDS (Sodium Dodecyl Sulfate) solutions as working fluid. The vertical test tube had a diameter of 19 mm and was 3.0 m long. For the bubbly and slug flow regimes, lower boundary values were found compared to those of pure water. However, for churn and annular flow regimes with surfactants, this effect was not found. Pressure measurements did show an effect due to the surfactant: in the churn-slug flow regime, there was a large reduction in the pressure gradient.

Xia and Chai (2014) [7] investigated the influence of surfactant on two-phase flow regimes and pressure drops in upward inclined pipes. Like Duangprasert et al., a 100 ppm SDS solution was used with a 11 m long Plexiglass® pipe of 59 [mm] in diameter. This research does not include entirely horizontal flows, though inclined flows were investigated up to angles of 15 ° from the horizontal position. The results show large influences of the surfactant on the reduction of the pressure gradient in both slug and annular flow regimes.

Liu et al. (2014) [11] used a 5.6 m vertical Plexiglass® pipe with a 40 mm diameter. The surfactant additive was HY-3, with a concentration of 1000 ppm. Main findings included a pressure drop reduction of up to 96.5 % caused by the surfactant, mostly pronounced in the slug flow regime. Also a liquid holdup reduction of up to 88.6 % was found in churn flow induced by the surfactant additive. Results also show that surfactant do not have a considerable impact on the transition of the two-phase flow, though they do have impact on the configurations of these two-phase flows.

Van Nimwegen (2015) [1] performed the most recent experiments on an air-water flow facility at Delft University of Technology. The set-up consisted of a 50 mm flow loop with a length of 12.5 m. The surfactant used was Trifoam 820 Block at a concentration range of 0-3000 ppm. Van Nimwegen considered the hydrodynamics of the flow with and without surfactant by visualization, and the effect of foam on the flow patterns and flow morphology. The type of surfactant, the inclination of the pipe and the pipe diameter were also investigated. Results have shown the following: the transition between churn and annular flow shifts towards lower gas flow rates when surfactants are used. This is because the foam decreases the density and changes the balance between interfacial friction and gravitational forces. Also, reductions in the pressure gradient were found, mostly pronounced at low gas flow rates. The optimum concentration of the surfactant was recognized by the value resulting in the lowest pressure gradient. The optimum concentration increases with increasing pipe diameter and has a negative correlation with the inclination from the horizontal. In later research by Van Nimwegen, multiple surfactants were used, producing similar results when scaled to an effective concentration.

As explained above, most research has been done on vertical (or upward inclined) pipe flows, though horizontal multiphase flows with surfactants are less well understood. So far, it is still unknown what effect surfactants have on horizontal flows with respect to slugging and flow stabilization. Therefore, one can conclude that there is room for development in the understanding of the effect of surfactants for these specific multiphase flows.

1.4. Outline of the report

The structure of the document is as follows: Chapter 2 discusses the fundamentals of multiphase flows which include the governing equations, the multiphase flow regimes, the different types of slugging, non-dimensional flow analysis and the conversion of SI units to industry units. Chapter 3 discusses the surfactant properties, the application of surfactants and the way these can be modeled for two-phase flows. Chapter 4 discusses the experimental setup of the research in detail, including the geometry of both configurations, control, intstrumentation and the type of surfactant. The results of the experiments are provided and analyzed in Chapter 5. Finally, Chapter 6 and Chapter 7 provide the conclusions and recommendations for further research.

Chapter 2

Fundamentals of multiphase flows

This chapter discusses two-phase air-water flows in pipelines. In the oil and gas industry, the most common multiphase flow is the simultaneous flow of hydrocarbon gas and hydrocarbon liquid through a reservoir, wells, transport pipelines, risers and facilities. This research focuses on multiphase liquid-gas flows, where the flow is measured in an air-water flow loop, operating at atmospheric pressure. The chapter starts with a discussion of the governing equations for two-phase flows. The general conservation laws can be derived to represent the conservation laws of two-phase flows. Next, the pressure drop along a pipeline is discussed. The pressure drop is shown in the TPC and is dominated by gravity or friction, depending on the airflow rate. Sec. 2.3 discusses the calculation of the liquid holdup. The next section discusses the existing flow regimes in detail, for upward vertical and horizontal flows. As this research focuses on slugging, Sec. 2.5 is dedicated to the different types of slugging encountered in pipelines and risers, including severe slugging and terrain slugs. The final two sections discuss the non-dimensional flow analysis and the conversion from SI units to industry units.

2.1. Governing equations for transport phenomena

The governing equations for transport phenomena include the equations for the transfer of mass, momentum and energy. These conservation laws hold for each of the phases in multiphase flows, given by:

$$\frac{\partial}{\partial t}\rho + \nabla \cdot \left(\rho u\right) = 0 \tag{2.1}$$

$$\frac{\partial}{\partial t}\rho \mathbf{u} + \nabla \cdot \left(\rho \mathbf{u} \otimes \mathbf{u}\right) = -\nabla \cdot p + \nabla \cdot \tau + \rho \mathbf{g} \tag{2.2}$$

$$\frac{\partial}{\partial t}\rho E + \nabla \cdot \left(\rho E \mathbf{u}\right) = -\nabla \cdot \left(\rho \mathbf{u}\right) + \nabla \cdot (\tau \cdot \mathbf{u}) - \nabla \cdot \mathbf{q} + \rho \mathbf{g} \cdot \mathbf{u} \tag{2.3}$$

Here, t denotes the time, ρ is the density and $\mathbf{u}$ is the fluid velocity. In Eq. 2.2 τ denotes the stress tensor. In Eq. 2.3, E is the total energy (sum of specific internal and specific kinetic energy) and q is the internal heat source.

2.2. Pressure drop

The pressure drop in a vertical pipeline is the force required to counter balance two forces: wall friction and gravity. The friction increases when the production rate is increased. The gravity force, which is also known as the hydrostatic head, is determined by the weight of the fluid in inclined pipe sections. In horizontal pipeflows, there is no pressure drop contribution of the hydrostatic head. At low production, the pressure drop in inclined sections is gravity-dominated, whereas at high production, the pressure drop is friction-dominated. This is schematically shown in Fig. 2.1.

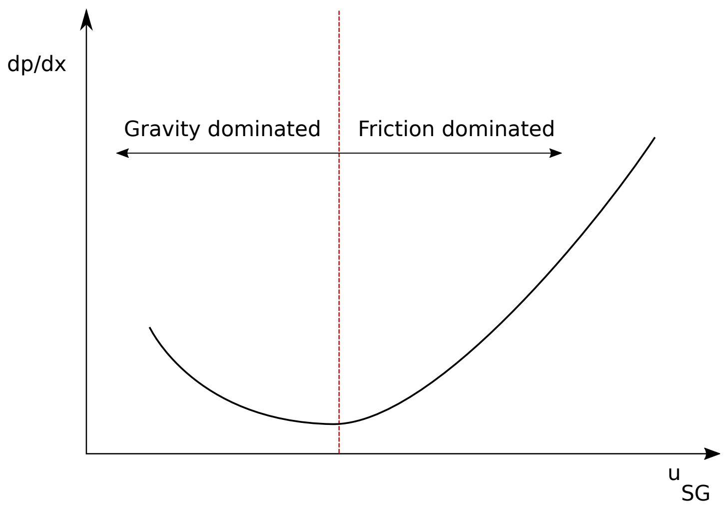

Figure 2.1: Pressure gradient plot as function of the superficial gas velocity for a vertical pipe flow. The superficial liquid velocity is constant.

To calculate the pressure drop along a two-phase flow in a pipeline, Newton's second law has to be applied to the liquid and the gas phase. Newton's law dictates the force balance including the pressure drop, acceleration of the flow, wall friction forces and gravity. Fig. 2.2 is a 1-D sketch of a two-phase flow in an upward inclined pipe section, where gravity is taken into account. The conservation of mass for the gas and liquid phases can be represented as follows:

$$\frac{\partial}{\partial t}\rho_G A_G + \frac{\partial}{\partial x}\rho_G A_G u_G = 0 \tag{2.4}$$

$$\frac{\partial}{\partial t}\rho_L A_L + \frac{\partial}{\partial x}\rho_L A_L u_L = 0 \tag{2.5}$$

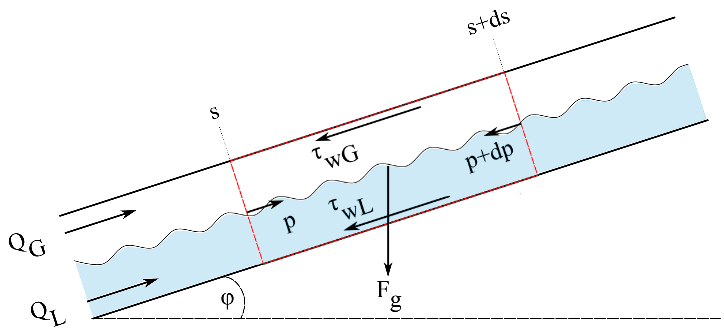

Figure 2.2: 1D representation of two-phase upward inclined flow

The momentum equations can be represented as follows:

$$\frac{\partial}{\partial t}\rho_G A_G u_G + \frac{\partial}{\partial x}\rho_G A_G u_G^2 = -A_G\frac{\partial P}{\partial x} + \tau_{wG}S_G - \rho_G A_G g sin(\varphi) \tag{2.6}$$

$$\frac{\partial}{\partial t}\rho_L A_L u_L + \frac{\partial}{\partial x}\rho_L A_L u_L^2 = -A_L\frac{\partial P}{\partial x} + \tau_{wL}S_L - \rho_L A_L g sin(\varphi) \tag{2.7}$$

Here, the subscript "G" denotes the gas phase and "L" denotes the liquid phase. A is the cross sectional area of the pipe section, x is the streamwise coordinate and τ is the wall friction of a certain phase (τ_{wG} and τ_{wL}). S is the wall perimeter wetted by a certain phase. The last two terms represent the gravity forces.

If the flow is assumed to be steady state, the time dependent contributions disappear from the mass and momentum equations. If the flow is also assumed to be fully developed, all streamwise (i.e. x) derivatives disappear, except for the pressure contribution. The gravity terms can be rewritten to gravitational forces. The momentum equations can be combined for both phases and simplified to:

$$-A\frac{\partial P}{\partial x} + \tau_{wG}S_G + \tau_{wL}S_L + F_{g,G} + F_{g,L} = 0 \tag{2.8}$$

Based on the flow pattern, the pressure drop can also be calculated by a mechanistic model. These mechanistic models consist of simplified momentum equations, and closure relations which are described in corresponding submodels. Tab. 2.1 provides an overview of the existing models and submodels, used to calculate the pressure drop. It is out of scope of this research to give a full explanation of the models stated in the table. The reader will therefore be referred to the textbook of e.g. Brennen [5].

2.3. Liquid holdup

The velocity of the gas and liquid phase can be described by a parameter called the superficial velocity (u_{SG} and u_{SL}). This velocity is equal to the velocity if the phase would flow alone in the pipe covering the full cross section. The superficial velocities are equal to the volumetric flow rate Q of the phase divided by the cross sectional area A of the pipe:

$$u_{SG} = \frac{\dot{m}_G}{\rho_G A} = \frac{Q_G}{A} \qquad u_{SL} = \frac{\dot{m}_L}{\rho_L A} = \frac{Q_L}{A} \tag{2.9}$$

By combining both superficial velocities for the liquid and the gas, one obtains the mixture velocity:

$$u_m = u_{SG} + u_{SL} \tag{2.10}$$

The phase volume fraction is defined as:

$$\lambda_L = \frac{u_{SL}}{u_{SL}+u_{SG}} = \frac{Q_L}{Q_L+Q_G} \qquad \lambda_G = \frac{u_{SG}}{u_{SL}+u_{SG}} = \frac{Q_G}{Q_L+Q_G} \tag{2.11}$$

Table 2.1: Classification of the mechanistic models and sub-models to calculate the pressure drop in two-phase flows [21]

Flow pattern	Models and submodels
Dispersed bubble flow	*Drift-flux model:* - Wall friction - Distribution parameter - Bubble rise velocity
Separated flow (stratified/annular)	*Two-fluid model:* - Wall friction - Interfacial friction - Interfacial velocity - Interface shape - Liquid entrainment
Intermittent flow	*Drift-flux & Two-fluid model:* - Wall friction - Distribution parameter - Bubble rise velocity - Void fraction in liquid slug body - Slug frequency - Length of liquid slug with gas bubble - Bubble shape

Where the phase volume fractions are coupled by: $\lambda_L + \lambda_G = 1$. The gas and liquid holdup is defined as the cross sectional area occupied by the phases divided by the total area.

$$\alpha_G = \frac{A_G}{A} \qquad \alpha_L = \frac{A_L}{A} \tag{2.12}$$

Again, both holdups together give: $\alpha_G + \alpha_L = 1$. The holdup is distinct from the phase volume fraction. This is because [16]:

- Gravity pulls the liquid downwards, resulting in a lower liquid velocity than the gas velocity in vertical (or upward inclined) pipe flows. There is a tendency for the liquid to accumulate, i.e. an increase in liquid holdup. On the contrary, for downward inclined pipe flows, the liquid will reach a higher velocity than the gas velocity
- A pressure force will act when the liquid viscosity is larger than the gas viscosity. This gives the gas a larger velocity than the liquid velocity, and causes a slip between both phases. This slip is not caused by gravity, and thus is present in both vertical and horizontal pipe sections. There is also an interfacial stress which appears at the liquid and gas interface. An increase in gas velocity will therefore tend to increase the liquid velocity as well. The higher the liquid velocity (at fixed liquid production) will decrease the liquid holdup

In addition to Fig. 2.1, we can conclude the following on liquid holdups. Low gas productions leads to a gravity dominated flow. This comes along with high liquid holdups in upward inclined flows, and low liquid holdups in downward inclined flows. Large gas productions leads to a friction dominated flow. The liquid will flow with the fast flowing gas, resulting in a low liquid holdup. The local liquid holdup fraction will be close to the liquid volume fraction (λ_l), due to a reduced slip between the gas and liquid phase. In case of a fully mixed gas and liquid phase, no slip exists between the phases. The liquid holdup fraction then equals the liquid volume fraction.

2.4. Flow regimes

In two-phase flow, one can distinguish four flow regimes in both vertical upward and horizontal flows. These patterns depend on physical, operational and geometrical parameters. Physical parameters which influence the flow pattern include the surface tension and gravity. Surface tension tends to make small gas and liquid bubbles spherical, and keeps pipe walls wet. Gravity pulls the heavier phase (liquid) down, especially in vertical flows. The operational parameters which influence the regimes are the flow rates of the liquid and gas phase. Geometrical influences stem from inclinations, wall roughness and the diameter of the tube [1][24].

In vertical upward flows, the following four flow regimes are observed for increasing gas flow rates, as shown in Fig. 2.3:

- Bubbly flow: gas bubbles have approximately a uniform size and move upwards in the liquid
- Slug flow: large bullet-shaped gas bubbles, known as Taylor bubbles, separated by liquid cylinders. The liquid contains small gas bubbles
- Churn flow: the liquid near the wall pulses up and down which results in a highly unstable flow of oscillatory nature
- Annular flow: the flow regime with the highest gas amount, in which the liquid is located as a film on the pipe wall. Small droplets are entrained in the gas core

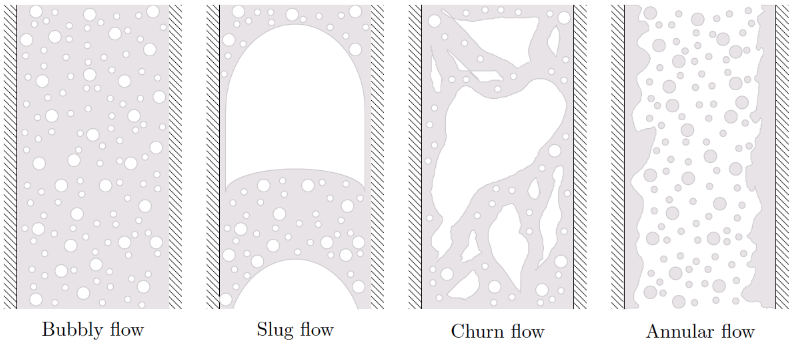

Figure 2.3: Flow regimes for vertical upflow in a tube [9]

Horizontal flows have similar flow regimes, though due to gravity they differ from vertical flow regimes. The axi-symmetrical behavior does not apply in horizontal flows, and the lightest phase is generally found on top of the heavier one, as shown in Fig. 2.4. Again, for increasing gas flow rates, the four regimes are:

- Dispersed bubble: high liquid flow rates and low gas flow rates result in small dispersed gas bubbles in the liquid core, which tend to flow in the upper part of the tube
- Slug flow: gas pockets interspersed with liquid slugs containing small gas bubbles
- Stratified flow: wavy liquid flows along the bottom of the pipe. The wave amplitude increases with the gas velocity. The gas contains small droplets of the liquid
- Annular dispersed: high gas flow rates push the liquid against the entire pipe wall, though due to gravity the amount of liquid on the bottom is higher. The gas core may contain entrained liquid drops

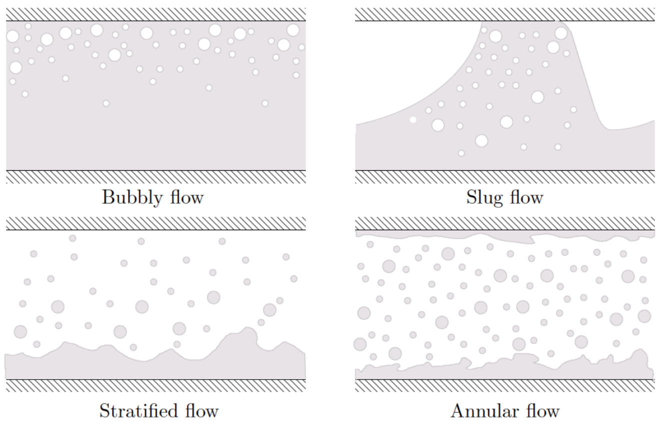

Figure 2.4: Flow regimes for horizontal flow in a tube [9]

The flow regimes can be plotted against the superficial velocity (for given fluids, inclination, pipe diameter), in a flow pattern map. Fig. 2.5 shows such maps for vertical upward flows (left) and horizontal flows (right). The axes show the supericial velocities of the liquid and the gas phase.

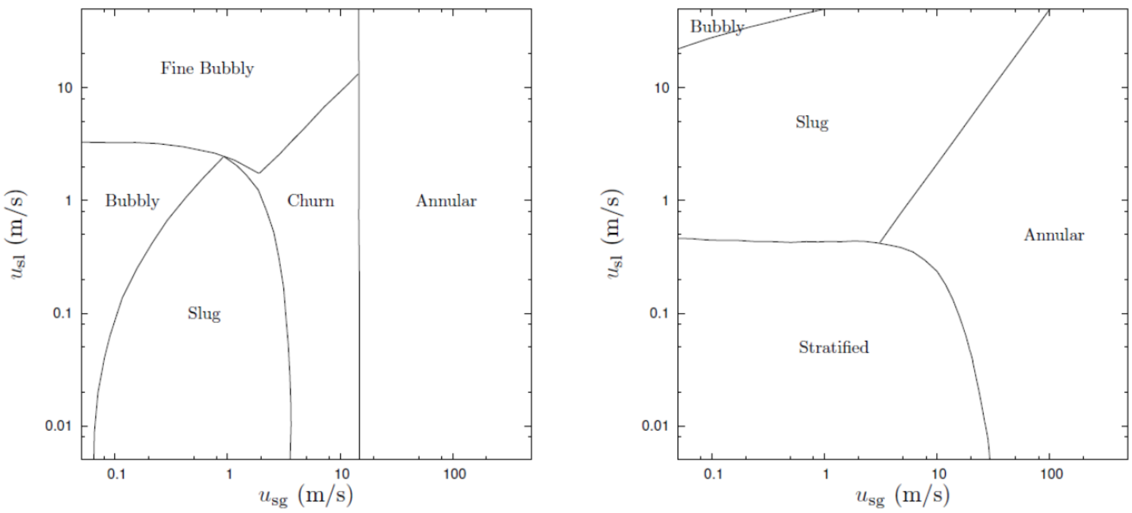

Figure 2.5: Flow pattern map for air-water flow, at atmospheric conditions, T_{amb} = 25 ° and diameter, D = 0.05 m [9]

The Shell Flow Explorer (SFE) simulation tool can be used to predict the flow regime and make flow pattern maps. The software package interfaces with the Shell Flow Correclations (SFC) engine to compute the characteristics of multiphase flows. The application is designed to simulate flows in a single pipe segment. Required inputs are the superficial velocities of the gas and liquid phases, density, viscosity, pipe diameter and surface tension. The results include the flow pattern map, the pressure gradient, and the liquid holdup fraction amongst others. Fig. 2.6 shows the decision tree which is used by SFE in order to compute the right flow regime.

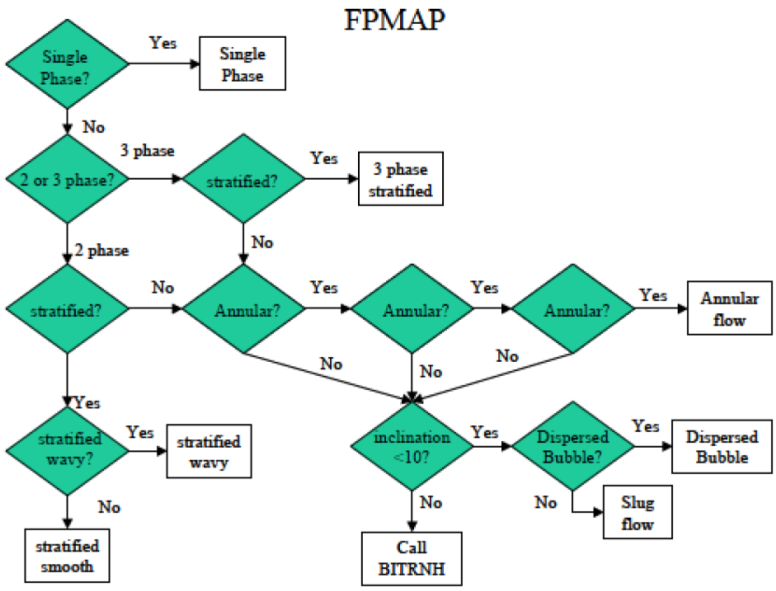

Figure 2.6: Shell Flow Explorer decision tree for the flow pattern [18]

2.5. Slug types

In a gas production system, the upstream boundary conditions are defined by the gas and liquid (condensate and water) mass flow rates, and the downstream boundary conditions by the separator pressure. Even though the boundary conditions are constant, an unsteady state flow may appear in wells. The phenomenon of large pressure amplitude fluctuations is known as severe slugging, and occurs at relatively low gas and liquid flow rates. Most production systems include horizontal, downhill and uphill sections. The varying geometry might also cause slug flows. In general, a distinction can be made between two types of slugging in a production system: severe slugging and transient slugging (including terrain slugging, hydrodynamic slugging and pig-generated slugging). In this research, we look at three types of slugging which might appear in the flow loop:

- Slugging in the flowline
- Slugging in the riser
- Sever slugging, also referred to as riser-based slugging

2.5.1. Slugging in the flowline

When water and air have a relative velocity, the interface may become unstable. This is caused by an imbalance of the destabilizing effect of inertia, over the stabilizing effect of gravity. It is known as the Kelvin-Helmoltz instability and plays an important role in two-phase flow regime characterization. The Kelvin-Helmoltz instability creates small waves at the gas-liquid interface, when there is a relative velocity. Gravity acts as a stabilizing force, trying to restore the interface. In an unstable situation, the amplitude of the interfacial waves will increase, and ultimately form a blockage across the entire cross section of the line. The flow will travel downstream as a slug, as shown in Fig. 2.4. In horizontal flows, the gas pockets will appear on top of the liquid film due to gravity.

2.5.2. Slugging in the riser

Slugging can also appear in vertical pipeflows. As gravity acts differently on vertical flows compared to horizontal ones, the flow in a riser is axi-symmetric. This means that the gas pocket, known as the Taylor bubble is located in the middle of the piping. Liquid is located in between these pockets, and as a film along the pipe wall. Fig. 2.3 shows the slugging regime in a riser.

2.5.3. Severe slugging

Severe slugging is a phenomenon related to liquid blockage initiated at the riser base, as shown in Fig. 2.7. This form of slugging is more pronounced when the upstream pipeline has a downhill inclination [15]. Severe slugging is characterized by a cyclic behavior. The cycle time ranges from a few minutes to a few hours. As depicted in Fig. 2.8, the cycle starts with a long period of neither gas nor liquid production at the top of the riser. This is followed by the arrival of a liquid slug. The length of this slug is longer than the riser height. Finally, a strong gas surge blows the slug through the riser. The cycle consists of five characteristics [16], shown in Fig. 2.7:

a) Blockage of riser base: severe slugging is initiated at low production. The riser operates in the hydrodynamic slugging regime, resulting in liquid falling back and block the riser

b) Slug growth: as liquids accumulate, the slug grows in the upward direction of the riser and upstream in the flowline. There is no production at the top of the riser. Gas builds up pressure upstream of the slug

c) Liquid production: once the entire riser is filled with liquid, the slug reaches the top and production at the separator starts

d) Fast liquid production: the tail of the slug in the pipeline reaches the riser base. The hydrostatic head in the riser starts to decrease, which in turn causes accelerated liquid production at the top of the riser

e) Gas blow-down: when all liquid has been produced at the top, the excess gas is released

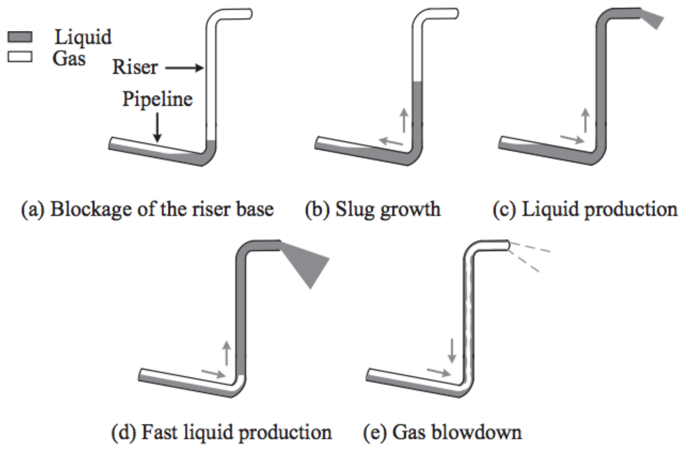

Figure 2.7: Severe slugging stages [15]

These five characteristics are also visible in the cyclic behavior of severe slugging, as denoted in Fig. 2.8. The figure shows a maximum pressure built up of 1.6 bar. This corresponds to a water column filling the entire riser of 16.8 m.

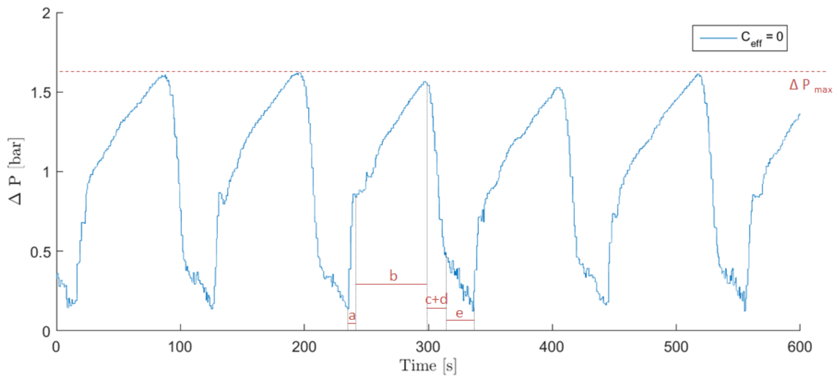

Figure 2.8: Severe slugging cycle on the SSL

Severe slugging occurs if the following conditions are satisfied [16]:

Condition 1
The Severe Slugging number Π_{SS} needs to be smaller than 1. This condition is also known as the Bøe criterion:

$$\Pi_{SS} = \frac{\left(\frac{dp}{dt}\right)_{flowline}}{\left(\frac{dp}{dt}\right)_{riser}} = \frac{P_0}{(1-\alpha_f)\rho_L g L_F} GLR < 1 \tag{2.13}$$

Here, P_0 is the pressure at standard conditions (Pa), α_f is the liquid holdup fraction in the pipeline upstream of the riser base (−), ρ_L is the liquid density (kg/m^3), L_F is the length of the pipeline upstream of the riser base (m), g is the gravitational acceleration (m/s^2) and GLR is the gas-to-liquid ratio at standard conditions (m^3/m^3). For the derivation of this equation, the following assumptions where made: (i) the riser is vertical, (ii) the riser and pipeline upstream of the riser have the same diameter, and (iii) $\rho_g << \rho_L$.

Condition 2
At the riser base, the flowline must reach a low point, where liquid blockage may occur.

Condition 3
The flowline must be operated in one of the following flow regimes: stratified or annular flow.

Condition 4
The flow in the riser is unstable, i.e. a higher pressure drop will be seen when a decrease in production occurs. This occurs when in the pressure drop is gravity dominated, as shown in Fig.2.1 in Sec. 2.2. A criterion with the densimetric gas Froude number gives a rough indication for the onset of unstable flow:

$$Fr_G^* = \sqrt{\frac{\rho_G}{(\rho_L - \rho_G)} \frac{V_{SG}^2}{gD}} < 1 \tag{2.14}$$

When the above mentioned four conditions are met, a severe slugging cycle will be obtained. The cycle can be described by the estimated length of the liquid slug and the cycle time:

$$L_l = \frac{L_R}{\Pi_{SS}} \tag{2.15}$$

$$\delta t = \frac{L_R}{u_{SL0}} \frac{1}{\Pi_{SS}} \tag{2.16}$$

Here, L_R is the height of the riser and u_{SL0} is the superficial liquid velocity in the pipeline at standard conditions.

Severe slugging typically occurs at late field life, when the GLR is low. It causes an unsteady production at the surface, and causes problems to the platform facilities. Problems are usually faced with separators, pumps and compressors, which are designed to operate at steady conditions. The severe slugging may cause over-pressurization, ruptures of the pipe, flooding and it increases the back pressure at the well head. It is therefore necessary to accurately predict the characteristics of the slugs, such as the length and the periodicity, when designing and operating a two-phase system.

2.6. Non-dimensional flow analysis

For single-phase flows, literature has shown that only two dimensionless numbers are needed to fully describe the flow characteristics and pressure distribution: the Reynolds number and the Froude number [21]. A two-phase flow (without mass or heat transfer) requires 10 parameters to describe the flow, as tabulated in Tab. 2.2 A derivation can be made in order to come to the minimum amount of dimensionless numbers

Table 2.2: Parameters used for non-dimensional flow analysis

Parameter	Symbol	Units
Gas velocity	u_G	m/s
Liquid velocity	u_L	m/s
Characteristic length	L	m
Gas density	ρ_G	kg/m^3
Liquid density	ρ_L	kg/m^3
Gas viscosity	μ_G	kg/(s· m)
Liquid viscosity	μ_L	kg/(s· m)
Surface tension	σ	N/m
Gravity constant	g	m/s^2
Pressure	P	N/m^2

needed to fully describe an isothermal gas-liquid two-phase flow without mass transfer. The equation of state, the conservation equations and the boundary conditions lead to a total of 6 dimensionless numbers [21], described by the 10 parameters as listed in Tab. 2.2. The liquid Reynolds number, which is the ratio fo inertia and viscous forces. It characterizes the change from laminar to turbulent flow:

$$Re_L = \frac{L\rho_L U}{\mu_L} \tag{2.17}$$

The Froude number, the ratio of inertial and gravitational forces:

$$Fr = \frac{U^2}{gL} \tag{2.18}$$

The Weber number, the ratio of inertial forces and surface tension:

$$We = \frac{L\rho_L U^2}{\sigma} \tag{2.19}$$

The Euler number, the ratio between pressure forces and inertial forces:

$$Eu = \frac{P_G}{\rho_G U^2} \tag{2.20}$$

The dimensionless gas density:

$$\widetilde{\rho_G} = \frac{\rho_G}{\rho_L} \tag{2.21}$$

The dimensionless gas viscosity:

$$\widetilde{\mu_G} = \frac{\mu_G}{L\rho_L U} = \frac{\mu_G}{\mu_L} \cdot \frac{1}{Re_L} \tag{2.22}$$

In case the above mentioned 6 dimensionless numbers are equal for two flow conditions, one can conclude the two systems to be identical.

2.7. Conversion of units

In the oil and gas sector, the liquid-to-gas ratio (LGR) is used to assess the type of field; mostly oil, water or gas. For air-water flows in a flow loop, this number can be computed as well. The gas-to-liquid ratio (GLR), the inverse of LGR, is more often used in experimental setups. GLR is given by:

$$GLR = \frac{Q_{gas}}{Q_{liquid}} = \frac{Q_{water} + Q_{condensate}}{Q_{gas}} \tag{2.23}$$

By using the above equation for this research, the air flow rates are given in normal cubic meters per hour (Nm^3/hr). Normal conditions for the gas are taken at a temperature of 293.15 K and 1.01325 bar. The water flow rate is in cubic meters per hour (m^3/hr). The GLR is a non-dimensional number.

However, in the oil and gas industry, the most common unit that is used is 'barrels per million standard cubic feet' (bbl/MMscf). Standard conditions for the gas are taken at a temperature of 273.15 K and 1 bar. Eq. 2.24 gives the conversion formula, from SI units towards industry units:

$$LGR \left[\frac{bbl}{MMscf} \right] = 6.2467 \cdot 10^7 \frac{T}{P} LGR \left[\frac{m^3}{m^3} \right] \tag{2.24}$$

Here, T stands for the temperature (K) and P for the pressure (Pa) of the liquid and gas mixture.

Chapter 3

Surfactants in two-phase flows

This chapter discusses surfactants and the foam they create in two-phase flows. The first section discusses the properties of surfactants. Surfactants decrease the surface tension of the air-water surface. Sec. 3.2 is dedicated to the application of surfactants. For the application in the oil and gas industry, a surfactant must have certain characteristics, which will be given. Sec. 3.3 discusses the way two-phase flows with surfactants can be modeled. A basic film model has been incorporated in the Shell Flow Correlations, enabling modeling of vertical and upward inclined flows with foam.

3.1. Surfactant properties

A surfactant molecule consists of a hydrophobic tail and a hydrophilic head. When added to water in an air-water mixture, the head will absorb into the water interface, leaving the tail in the air phase. Increasing the concentration of the surfactant increases the amount of molecules absorbed in the air-water interface. It results in a reduction of surface tension by a factor of 2-3 [12]. This phenomenon is seen up to a critical micelle concentration (cmc). When the cmc is reached, the entire air-water interface has been covered by surfactant molecules, and other surfactant molecules start to form micelles. These are groups of molecules, where the hydrophobic tails are enclosed by the hydrophilic heads. When micelles start to form, the surface tension no longer decreases with increasing surfactant concentration. This is illustrated in Fig. 3.1.

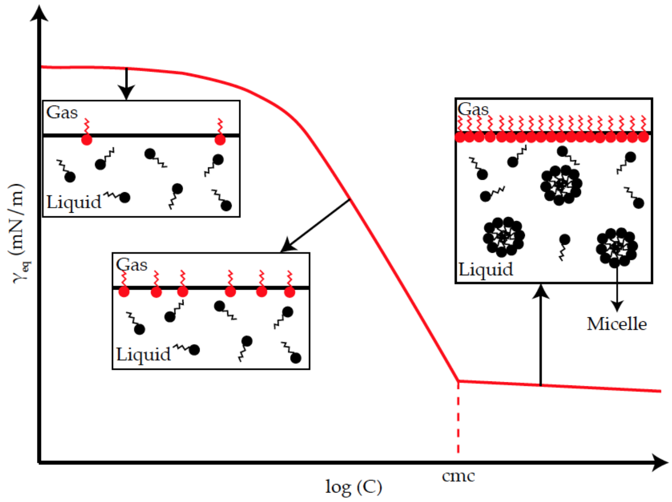

Figure 3.1: Decreasing surface tension with increasing surfactant concentration, up to the critical micelle concentration [1]

When a surfactant is added to an air-water mixture, the surface tension is initially equal to the surface tension of just water and air (72 [mN/m]). It takes time for the surfactant to first diffuse through the water, and second to be absorbed into the interface. The diffusion rate and the rate of the absorption process are therefore related to the surface tension: it decreases over time. This effect is known as the dynamic surface tension, as illustrated in Fig. 3.2.

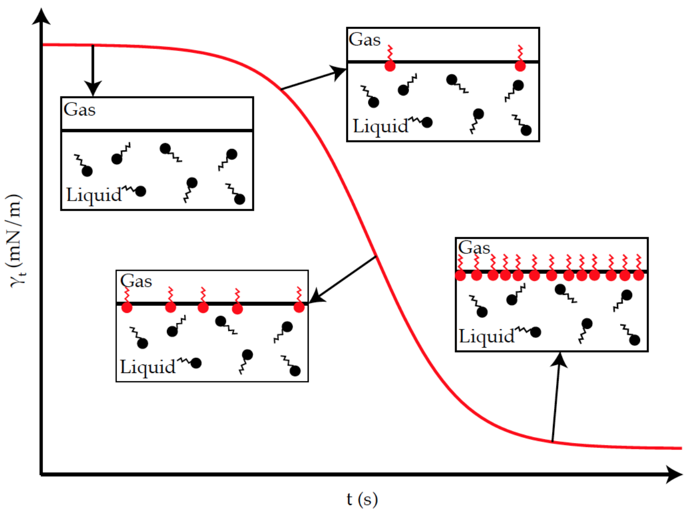

Figure 3.2: Time-dependency of the surface tension: dynamic surface tension [1]

Surfactants can create dispersed gas pockets in a liquid, known as foam. In order to create foam, some form of agitation is needed, such as shaking, rotating or sparging. Once sufficiently agitated, and added above a certain concentration, the surfactant will create a foam. The gas forms bubbles within a network of small liquid films. It is the dynamics of the surface tension which allows the surfactant to form a stable foam. When a foam bubble forms, the film around the gas pocket is stretched and becomes thinner. The surface area increases, which decreases the concentration of the surfactant. As seen in Fig. 3.2, a lower concentration leads to a higher surface tension locally in the film, causing a surface tension gradient. The surface tension gradient is pulled along the liquid film over the foam bubble. This stabilizes the bubble constantly [20]. Pure liquids never foam, because the liquid films are not stabilized this way. The liquid films in pure water will rupture directly, avoiding the formation of a stable foam.

3.2. The application of surfactants

The foam created by a surfactant has a wide variety of applications. It is used in building material, used as soap in domestic environments and used in engineering processes, such as in the gas and oil industry. Each application encounters a different length scale of the foam, as illustrated in Fig. 3.3.

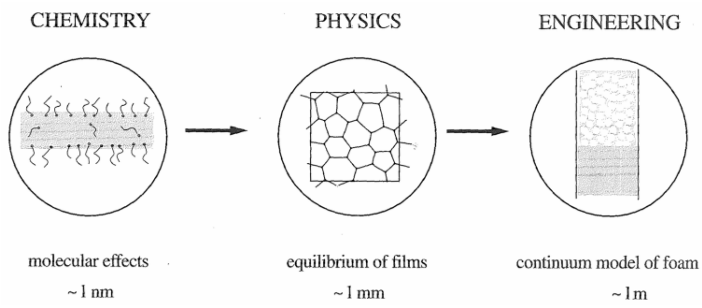

Figure 3.3: Length scales of foams and their applications [1]

In the oil and gas industry, surfactants are used for the deliquification of gas wells. This is done by either preventing the formation of slugs, or to mitigate the impact of the slugs. First a suitable surfactant has to be found. This is done by bench top lab testing. Gas wells come with different geometries, pressures, temperatures, and compositions of the product. It is therefore necessary to select a surfactant suitable to a specific well, which creates a foam with the desired criteria. In general, to increase production rates, the applied foam should be:

- *Stable and long lasting* - if this is the case, the surfactant can be injected in batches, and re-injected once the foam has collapsed
- *Able to foam in a water/condensate mixture* - the gas flowing towards the surface face a large decrease in temperature. Condensate of the gas is therefore present. Also, water from the field flows through the pipeline systems along with the gas. The surfactant should therefore be able to cope with these two liquids, to create a foam
- *Self-agitating* - to simplify the process of using surfactants, self-agitating surfactants are used, such that shaking, rotating or sparging is unnecessary. Self-agitating surfactants contain a chemical agitator
- *Effective in presence of small volumes of condensate and hydrate inhibitors*
- *Show no adverse effects on-shore in downstream processes* - as the foam will arrive at the surface facilities along with the product, it is important it has no negative effects on either the product, the facilities, or the environment
- *Able to anti-foam* - Foam might affect the facilities when it arrives on-shore in large volumes. Also, it might be necessary to break down the foam earlier in the process during downtime for e.g. inspection. It is therefore preferred to pick a surfactant which anti-foams fast and easily.
- *Does not tend to form emulsion* - emulsions complicate the process and this is therefore an undesired phenomenon

Once a surfactant is selected, it is ready to be injected down hole in the well. This can either be done continuously or in batches. The surfactant will down hole create a foam.

The foam has a large volume, a low density, and a large viscosity compared to the trapped liquids in the well. The hydrostatic head is reduced when mixing the foam with the liquids down hole. It is therefore possible to lift the water-condensate-foam mixture to the surface and prevent liquid loading.

3.3. Modeling two-phase flow with surfactant

The modeling of two-phase flows with surfactants can be done through the Shell Flow Correlations (SFC). Since 2016, the film model has been added, which is available for vertical and upward inclined flows. It is based on the model as discussed by Van Nimwegen, Portela and Henkes (2017) [3]. Apart from the fluid properties and the pipe diameter, there are three inputs required: the superficial gas velocity, the superficial liquid velocity and the effective surfactant concentration. The latter input will be discussed in more detail in Sec. 4.4. Through a bisection method, the correct value of the film thickness δ is found. The output consists of the pressure gradient, the thickness of the liquid and the foam layer in the film, and the foam density. The latter parameter is used to obtain the liquid and foam hold-up. A schematic of the calculations performed by the SFC for the film model is shown in Fig. 3.4.

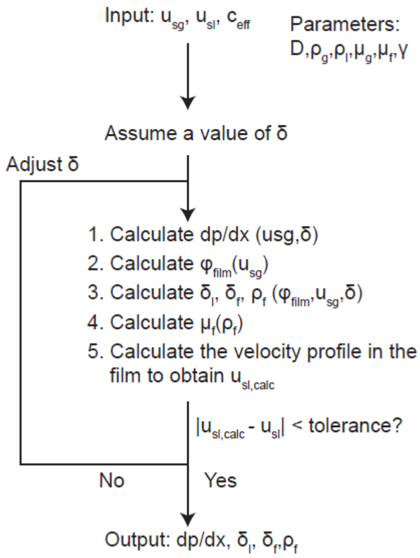

Figure 3.4: Schematic of the calculation steps taken by SFE through the film model [4]

The two-phase flow is modeled as an annular flow with surfactant. It does not take entrainment of liquid bubbles in the gas phase into account, as entrainment is suppressed by foam [1]. In annular flow, the pipe wall is covered by a liquid film. The film model consists of two layers, a liquid and a foam layer, based on flow visualizations that have been performed [1]:

$$\delta = \delta_f + \delta_l \tag{3.1}$$

An illustration of the layers and the gas core is shown in Fig. 3.5. In Fig. 3.5, u_{sl} indicates the superficial liquid velocity, u_{sg} is the superficial gas velocity, δ_l is the thickness of the liquid layer in the film, ρ_f is the foam density, ρ_{film} is the film density, μ_f is the foam viscosity, and f_i is the interfacial friction factor. The pressure gradient in the turbulent gas core is calculated as follows:

$$-\frac{\partial P}{\partial x} = \frac{4}{D-2\delta} f_i \frac{\rho_g (u_g - u_i)^2}{2} + \rho_g g \tag{3.2}$$

Here, P is the pressure, x is the streamwise coordinate, D is the pipe diameter, δ is the thickness of the film, f_i is the interfacial friction factor, ρ_g is the gas density, and u_i is the velocity of the gas-liquid interface. The gas velocity (u_g) is found by applying a correction to the superficial gas velocity (u_{sg}):

$$u_g = u_{sg} \frac{D^2}{(D-2\delta)^2} \tag{3.3}$$

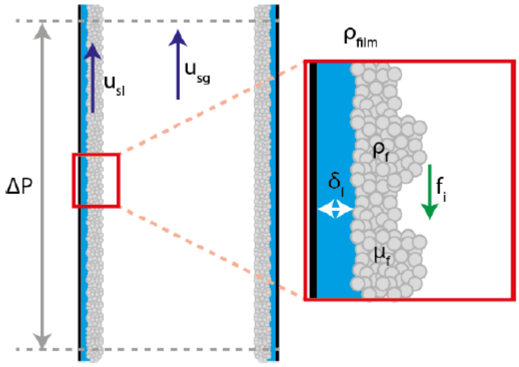

Figure 3.5: The basic concept of a film model [4]

Laminar flow is assumed for both the liquid and the foam layer. The foam is therefore considered as a non-Newtonian fluid. The velocity profile is obtained as follows:

$$\frac{1}{r}\frac{\partial}{\partial r}\left(r\frac{\delta u}{\delta r}\right)=\frac{1}{\mu}\frac{\partial P}{\partial x}-\rho g \tag{3.4}$$

Here, r is the radial coordinate, u is the velocity in the streamwise direction, and μ is the viscosity. The boundary conditions have to be specified to solve Eq. 3.4. For small radial coordinate, the velocity gradient is based on the interfacial friction. For the large radial coordinate, the velocity is set to a fixed value.

The boundary conditions for velocity of the liquid layer (u_l) are:

$$u_l|_{r=R}=0 \tag{3.5}$$

$$\frac{du_l}{dr}|_{r=R-\delta_l}=\frac{D-2\delta_w}{4\mu_l}\left(\frac{dP}{dx}-A\rho_g g-(1-A)\rho_f g\right) \tag{3.6}$$

A is a factor, and is given by:

$$A=\left(\frac{D-2\delta}{D-2\delta_l}\right)^2 \tag{3.7}$$

The boundary conditions for velocity of the foam layer (u_f) are:

$$u_f|_{r=R-\delta_l}=u_l|_{r=R-\delta_l} \tag{3.8}$$

$$\frac{du_f}{dr}|_{(r=R-\delta)}=\frac{D-2\delta}{4\mu_f}\left(-\frac{dP}{dx}-\rho_g g\right) \tag{3.9}$$

The next step in the calculation is the film density. Through the mass balance, one can obtain ρ_{film}:

$$V_{film}\rho_{film}=V_l\rho_l \tag{3.10}$$

Here, the V_{film} is the volume of the film (i.e. both the foam and liquid), V_l is the volume of the water and ρ_l is the density of the water. From the film density, the film liquid content (φ_{film}) can be calculated:

$$\varphi_{film}=\frac{\rho_{film}}{\rho_l} \tag{3.11}$$

The film density is used to calculate the thickness of the liquid and foam layers of the film. The assumptions made here are: (i) the liquid film has a minimum thickness of 10μ, and (ii) the foam liquid fraction is at most 34%. With the thicknesses, one can obtain the foam density (ρ_f) with the following equation:

$$\rho_{film}=\frac{D^2-(D-2\delta_l)^2}{D^2-(D-2\delta)^2}\rho_l+\frac{(D-2\delta_w)^2-(D-2\delta_l)^2}{D^2-(D-2\delta)^2}\rho_f \tag{3.12}$$

The foam properties are also taken into account in this model. The easiest way is to model the fluid as a Newtonian fluid, assuming a constant viscosity tensor. However, foam has a yield stress and is shear thinning. Foam is therefore usually modeled as a Hershel-Bulkley fluid [6], a generalized model of a non-Newtonian fluid, where the shear stress and shear rate are related in a complicated and non-linear way. The shear stress τ and the shear rate ∂u / ∂y are related as follows:

$$\tau = \tau_y + \mu_{hb} \left(\frac{\partial u}{\partial y} \right)^n \tag{3.13}$$

Here, τ_y is the yield stress, μ_{hb} the Bingham viscosity and n the shear index. For shear thinning fluids, the shear index $n < 1$. Thereby, an effective foam viscosity can be modeled as:

$$\mu_f = \frac{\tau}{\frac{\partial u}{\partial y}} \tag{3.14}$$

In the model described by van Nimwegen, Portela and Henkes (2017), the effective foam viscosity depends only on the liquid content of the foam. If the content is more than 34%, the foam behaves as a bubbly liquid without a yield stress. In order to have bubbles attached to each other, a lower liquid content is required [3].

Foam is complex, which results in a large variety in foam rheology. Currently, there is no model that takes into account all the factors influencing foam rheology such as the water content and internal structure. One of the complications for the internal structure is the liquid film which is formed along the wall. Bubbles are restricted at the wall, and have to be aligned there, forming a liquid film. Since the viscosity of water is much smaller than the viscosity of foam, the velocity gradient is mostly in the liquid layer. The slip layer therefore has a dominating effect on the foam velocity [2].

Chapter 4

Experimental setup

This chapter discusses the experimental setup of the research conducted at the Shell Technology Centre Amsterdam (STCA). It describes the geometry of the air-water flow facility, known as the Severe Slugging Loop. The flow loop consists of a 100 m flowline and a vertical riser with a length of 16.8 m. It is able to generate severe slugging, and is equipped with a Smart Choke controller (which has not been used in this study).

For this research, several modifications have been done in 2017. These include an air injection point at the riser base, and the installation of pressure sensors and quick closing valves on the riser. It is the first time surfactants are used in the Severe Slugging Loop. No extra modifications to the loop are required with respect to using surfactants in the air-water flow loop.

The chapter starts with a description of the flow loop geometry for both conducted experiments. It continues with the control, including flow meters, pressure sensors and quick closing valves. Then, the instrumentation is discussed including the Distributed Acoustic Sensors and the camera. The last section discusses the surfactant and the corresponding concentrations.

4.1. The flow loop

The Severe Slugging Loop was used for this research, located at the outside plot at STCA, as shown in Fig. 4.1. It is a flow loop where water and air can generate multiphase flows. The maximum pressure is 6 [bara]. The SSL can be operated from a computer in the porto cabin, located next to the setup. This is also the location where measurements can be recorded. For this research, two configurations of the SSL are used.

Figure 4.1: The Severe Slugging Loop located at STCA.

Configuration #1: water and air injection into the flowline

The first experiment makes use of the flowline which is connected to a riser, as shown in Fig. 4.2. Water and air are injected through a Y-sprout into a horizontal flowline. The flowline has a total length of 100 m and takes a bend halfway. It is made of galvanized steel segments, with an inner diameter of 0.051 m. It also contains transparent perspex segments with an inner diameter of 0.051 m. These segments are located just before the bend, and the last 32.1 m of the flowline connected to the riser base. Of the latter perspex segment, 26 m has a downward inclination of about 2 [degrees] from the horizontal. The flowline is connected to a vertical riser, with an inner diameter of 0.050 m. It is also made of transparent perspex. The riser has a height of 16.8 m. Once the mixture has reached the top, it enters a vessel (V-201). This vessel acts as a storage before the mixture falls down into the separator (V-202). Here, air and water are separated by gravity; air is vented to the atmosphere, water falls down and is pumped back into the flowline.

Configuration #2: air injection into the riser, water injection into the flowline

For the second experiment, a slightly different configuration of the SSL is used, as shown in Fig. 4.3. The loop can be modified with two hand valves, such that the air has an inflow point directly at the riser base. The water injection point is thereby not modified, and will still follow the flowline before entering the riser. In this configuration, water and air will start mixing at the riser base, instead of in the flowline as in the flowline and riser experiment. The control equipment and instrumentation have therefore been installed on the riser, including differential pressure indicators and quick closing valves (Sec. 4.2) and a camera (Sec. 4.3).

In Appendix B, more photos are shown of the layout of the loop and the control and instrumentation installed on it. The technical drawing of the Severe Slugging Loop is given in Appendix C.

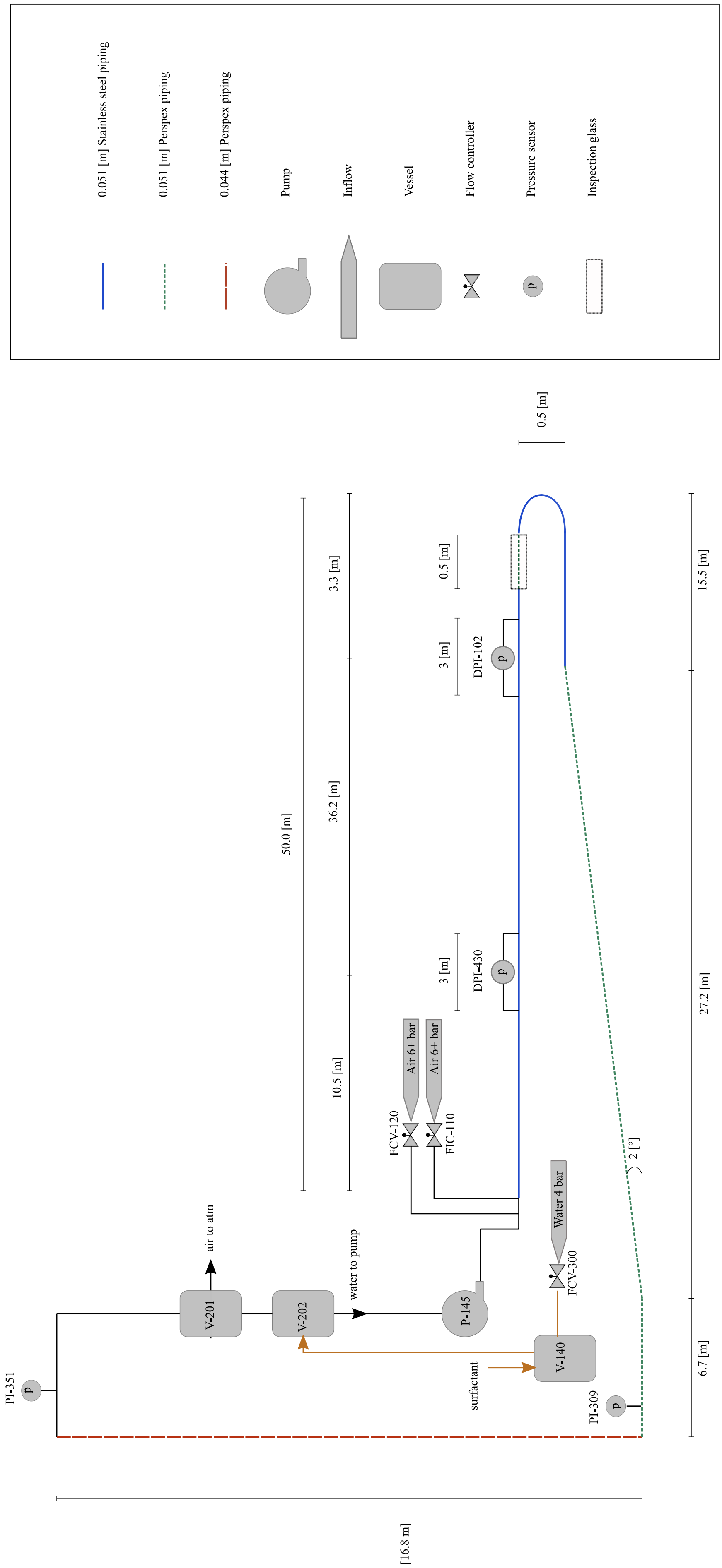

Figure 4.2: Schematic overview of configuration #1 of the SSL where both air and water are injected into the flowline

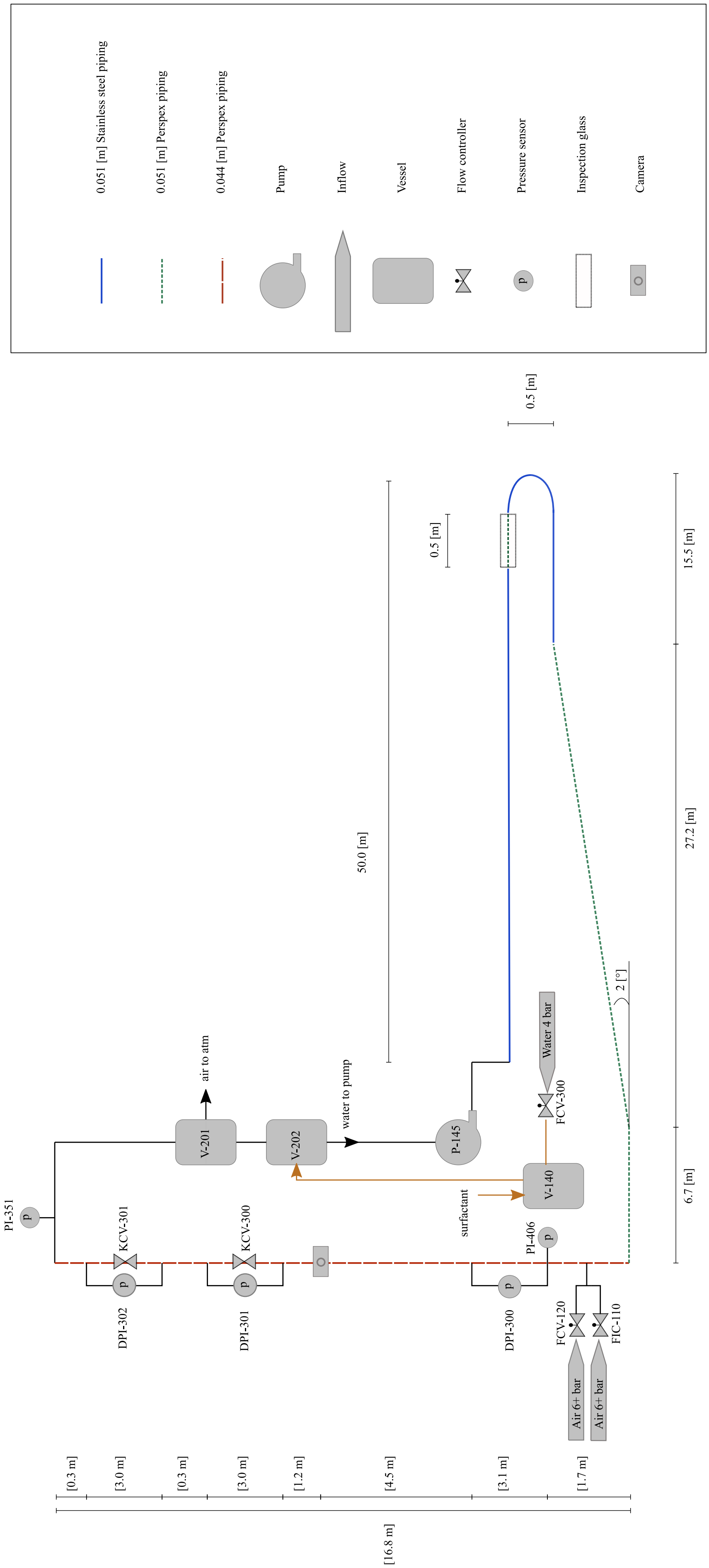

Figure 4.3: Schematic overview of configuration #2 of the SSL where water is injected into the flowline and air is injected into the riserbase

4.2. Control

The water and air which run through the pipelines of the SSL are controlled by flow meters, pressure sensors and quick closing valves.

4.2.1. Flow meters and control

The SSL runs with water and air, which are both controlled by flow controllers and monitored by mass flow indicators. Water, which is pumped into the flowline, passes a flow control valve (FCV-300) and a mass flow indicator (FI-300). The mass flow indicator is of type Endress + Hauser PROMAG50 with an accuracy of ± 0.5%.The SSL can operate over a range of water flow rates from 0.25 to 4.00 m^3/hr. As water can be assumed to be incompressible, one can directly calculate the superficial liquid velocities, by dividing the water flow rates by the cross sectional area. The superficial velocity range for the horizontal flowline is 0.03 to 0.54 m/s. The superficial velocity range for the vertical riser is 0.05 to 0.73 m/s.

The STCA air supply provides air at 6+ bara to the SSL. The air supply is controlled by two air flow controllers. For low air flow rates, the FIC-110 of type Brooks Instrument 5853E is used. It has a range of 0-48 Nm^3/hr. For large air flow rates, the flow control valve FCV-120 and mass flow indicator (FIC-120) are used. The mass flow indicator is of type Endress + Hauser PROline Prowirl 72, with an accuracy of± 1%. It has a range of 30-300 Nm^3/hr. Both mass flow controllers can be used simultaneously. As air is compressible, one has to take the operating pressure into account when calculating the superficial gas velocity (u_{SG}). For this conversion, one starts with the gas law:

$$\frac{P_1 u_1}{T_1} = \frac{P_2 u_2}{T_2} \tag{4.1}$$

Where P stands for the pressure, u the velocity and T the temperature. When defining subscript 1 as the normal conditions and subscript 2 as the actual conditions, this leads to:

$$u_{g,actual} = u_{g,normal} \left(\frac{P_{normal}}{P_{actual}} \right) \left(\frac{T_{actual}}{T_{normal}} \right) \tag{4.2}$$

Normal conditions are given for a gas at a temperature of 273.14 K and a pressure of 1 bar. The actual conditions are dependent on the conditions of the operation.

4.2.2. Pressure sensors

There are two types of pressure sensors used on the SSL: Pressure Indicators (PI) and Differential Pressure Indicators (DPI). PIs indicate the absolute pressure at one point in the loop. DPIs are two-legged pressure sensors, measuring the difference in pressure between two points. Along the SSL, several of these two instruments are installed.

On the flowline, a DPI (DPI-340) is located at 206 pipe diameters from the water and air inlet. The second DPI (DPI-102) is located at 920 pipe diameters from the inlet, which is just before the flowline takes a bend. The DPIs are connected to the flowline by two capillaries. The differential pressure is measured by a membrane inside the cell. The DPIs on the flowline measure the differential pressure over a 3 m distance. They are of type Endress+Hauser PMD7. The transmitter gives an output between 4-20 mA, which is converted into a pressure by the carrier demodulator. The DPIs have a nominal range of 0-100 mbar, though are calibrated to 0-50 mbar. For the lower region of the full range, i.e. 0-10 mbar, the accuracy is 2.2 % of the full range.

The vertical riser has 3 DPIs installed with a calibrated range of 300 mbar. The accuracy is 0.05 % of the nominal range of 500 mbar. The output signal varies between 4 and 20 mA. DPI-300 is located at a height of 3.3 m and measures the differential pressure over 3.1 m. DPI-301 is located at a height of 11.8 m. The third DPI, DPI-302 is located a height of 15.0 m. The latter DPIs measure the differential pressure over 3.0 m.

Furthermore, there are several pressure indicators installed. The flowline and riser setup makes use of a pressure indicator at the riser base (PI-309), and on at the top of the riser (PI-351). For the riser only configuration, a pressure indicator located just after the air injection at the riser base is used (PI-406). For safety reasons, another pressure indicator is installed at the beginning of the flowline (PI-300). This PI can be used as an indication of the system pressure, and should therefore not exceed the maximum operational pressure of 6 bara. The pressure indicators have a measuring range of 0-10 bar. The PIs are of type Endress+Hauser PMC41 and Endress+Hauser PMC51 (successor of PMC41) with an accuracy of ± 0.2%.

4.2.3. Quick closing valves

Two quick closing valves are installed on the riser, 3 m apart from each other (KCV-300 and KCV-301). The valves are ECON FIG. 7289 ball valves by Econosto. They consist of a pneumatic actuator, which is single acting and closed by a spring. By actuating the valves in the GUI, a single signal is sent out to the controller: the flow between the two valves will be shut. The actuation of the quick closing valves is coupled to the water pump and the air flow control valve. Both are shut simultaneously to prevent the system from over pressurizing upstream of the quick closing valves. Once the valves are shut, the holdup can be determined, by measuring the height of the water between the valves manually. If foam is present, the height of the liquid and foam is measured. A scale was attached to the riser, to determine the height. The quick closing valves are installed at a height of 11.8 m and 15.1 m (i.e. 236 and 302 pipe diameters) to ensure fully developed flow in the riser. Also, a distance of 1.8 m (i.e. 36 pipe diameters) is kept from the top of the riser, to avoid any effects of the bend at the riser top.

4.3. Instrumentation

The instrumentation used on the SSL include Distributed Acoustic Sensing and a camera.

4.3.1. Distributed Acoustic Sensing

The Distributed Acoustic Sensing (DAS) apparatus detects acoustic signals in the flowline. The acoustic signals make it possible to visualize the noisiness of the flow; it measures sound with the speed of light. The apparatus consists of a box (containing a laser with an interrogator) and a long fiber. The box is located in the porto cabin, as located next to the flow loop, with the beginning of the fiber connected to it. The rest of the fiber continues along the flowline. The laser emits a light pulse at 10 kHz with a typical wavelength of 1550 nm. The speed at which the light propagates through the fiber is given by:

$$v = \frac{c}{n} \tag{4.3}$$

Here, c denotes the speed of light and n the refractive index of the fiber. The speed of light in vacuum is $2.9977 \cdot 10^8$ m/s. The refractive index of the fiber is 1.5. As stated by Snell's Law, there will be total internal reflection of the light if 1) the core of the optical fiber has a larger refractive index than its surrounding cladding, and 2) the angle of incidence is smaller than the critical incidence angle. If this is the case, the light will be forced to propagate through the fiber, enabling the use of optical fibers for data transmission and sensing applications such as DAS.

Due to irregularities in the production of the fiber, the density of the fiber modulates slightly, causing inhomogeneities to exist. When a short light pulse travels through the fiber, the light is backscattered due to these inhomogeneities in the fiber. DAS makes use of Rayleigh backscatter, an elastic process in which the light is returned at approximately the same wavelength as the incident wave [13]. The interrogator analyses the backscattered spectrum. Slugs produce acoustic energy, which is absorbed by the molecules of the fiber material. Due to the absorption, a phase shift appears in the backscattered spectrum. The location of the slug is determined by measuring the time that has elapsed between the launching of the pulse and receipt of the backscattered light. This can be done due to a constant speed of light c and a changing velocity v. The time at which the backscattered light from dept z is captured by the interrogator is given by:

$$t = \frac{2z}{v} \tag{4.4}$$

The amplitude of the backscattered light is measured at fixed intervals, known as channels. Along the entire length of the fiber, a series of independent acoustic samples are taken. This is done by a certain spatial resolution, which is approximated by:

$$\delta z = \frac{v \delta t}{2} \approx 10^8 \cdot \delta t \tag{4.5}$$

Here, δt is the pulse duration, which has a value of 10 [ns]. For the experiments on the SSL, the spatial resolution is set to the smallest possible value, i.e. 1.0 m.

On the Severe Slugging Loop, 912 m of optical fiber are used. With a resolution of 1 m this corresponds to 912 channels. The fiber starts in the DAS box, and is mounted onto the flowline of the SSL. The fiber is wrapped 9 times along the flowline, as illustrated in Fig. 4.4. It runs from the top (2x), to the side (2x), to the bottom of the flowline (2x). At last it is wrapped along the top (1x), the side (1x) and bottom (1x) of the flowline. DAS equipment is very sensitive to temperature changes. It is therefore necessary to isolate the fiber optics, to minimize weather effects during the experiments.

Raw DAS data can be uploaded in OptaSense DxS Browser, a software which enables post-processing of

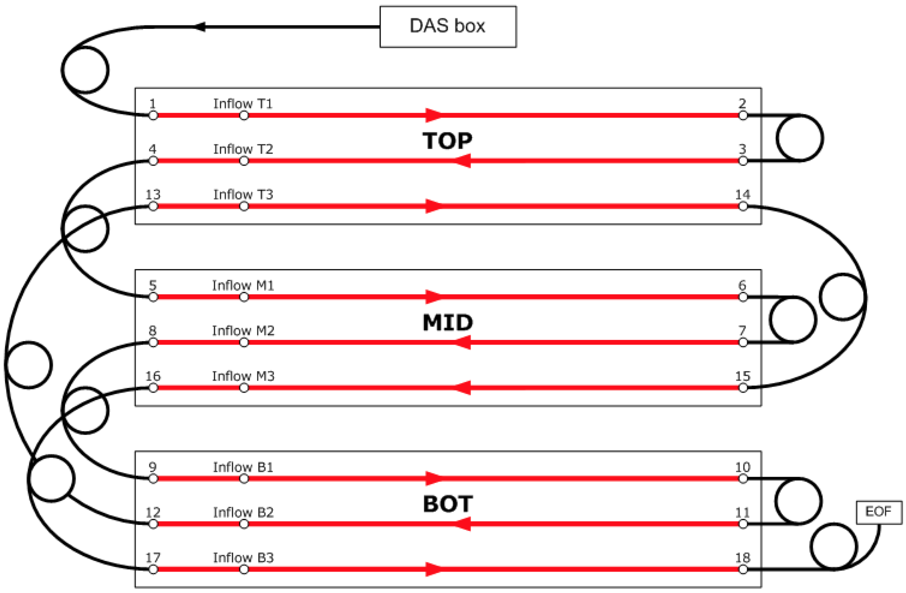

Figure 4.4: Layout of the DAS fiber wrapped 9x along the flowline: 3x along the top, 3x along the side and 3x along the bottom.

the data. The software can compute Fast Fourier Transform data (FFT) and Frequency Band Extracted (FBE) data. FFT data can be plotted in an intensity (dB) versus frequency (Hz) plot. This plot visualizes the signal, as detected in the flowline. From this plot, one can determine in which frequency bands the signal is located. Selecting these bands gives best results when visualizing FBE data. The downside of FFT data is that 15 min of raw DAS data leads to FFT data sizes of about 50 GB. To avoid long computing times, it is preferred to directly look at FBE data. FBE data can be post-processed in MATLAB to visualize the signal along the entire length of the fiber optics, as seen in Fig. 4.5. The length of the fiber is expressed in channels, as seen on the y-axis of the plot. A few of these channels can be selected to visualize e.g. only the fibers along the top of the flowline. In this case, the channels corresponding to the top of the flowline are 176-218, 256-298 and 653-695. As the fibers are wrapped along the flowline, channels #176-218 mirrors the signal of channels #256-298. The advantage of working with FBE data is that it is much smaller than FFT data. However, frequency band selection for best visualization is chosen by trial and error.

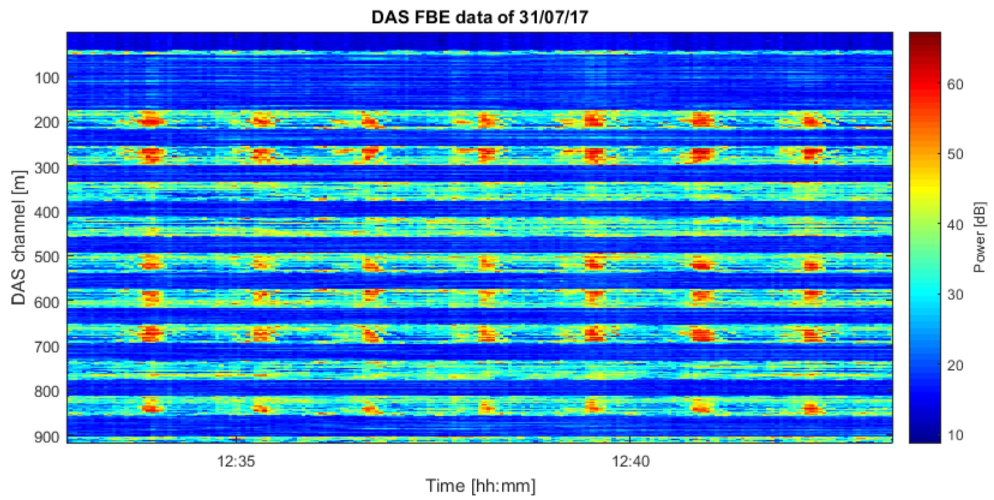

Figure 4.5: An FBE plot of DAS data, visualizing the acoustic signal along the fiber. The top of the plot (channel #0) corresponds to the DAS box, where the fiber begins. The fiber is then laid along the flowline 9 times, which is visualized by the 9 horizontal beams on the plot where an acoustic signal is detected.

.

4.3.2. Camera

The multiphase mixture can be seen through the perspex segments on the flowline and the riser. Besides visualization by the naked eye, a Go Pro™ HERO4 camera is installed on the riser at a height of 9 m, as indicated in Fig. 4.3. The shutter speed of the camera depends on the frame rate. A trade-off has to be made, as a high frame rate leads to a low resolution. The frame rate is set to 80 frames/s, corresponding to a resolution of 1080s p.

4.4. The surfactant

This research makes use of Dreft™ as the surfactant. Dreft™ is a dish washing detergent, owned by the multinational Proctor & Gamble™. The main reason to use Dreft™ is that it is safe. After having run through the air-water flow facility, the water containing the surfactant can be flushed down into the sewer. There is no need for post-treatment to reduce the toxicity. Although Dreft™ has not been used in wells before, it is a good representation of a foamer to be used in a water and air facility. Dreft™ does not need any safe storage.

4.4.1. Adding the surfactant to the system

During the experiments, the surfactant concentration is gradually increased. When doing so, the flowlines, riser, separator and water storage vessel underneath must first be emptied. The surfactant is then added to the large water vessel on the ground (V-140 in Fig. 4.2 and Fig. 4.3) and stirred by hand to distribute the surfactant uniformly through the water volume. The mixture is then pumped to the separator, and then into the flowlines to fill up the SSL again. The startup process is indicated by the orange lines in Fig. 4.2 and Fig. 4.3. The foam is formed through the hydrodynamics of the air-water flow in the flowline and riser. To remove the foam from the loop, the system is first drained entirely. Then extensive flushing with water is needed, to remove all surfactant remainders from the system.

4.4.2. Concentrations

The reference case is the experiment in which no surfactant is used (concentration of 0 ppm). Earlier performed research by Van Nimwegen [1], mentions an effective concentration. This is the concentration of a surfactant in water, which gives the same amount of foam, compared to multiphase flows containing the surfactant Trifoam. Other surfactants can be multiplied by a scaling factor (f_s) to find the effective concentration:

$$C_{eff} = f_s C \tag{4.6}$$

The scaling factor of Dreft™ is 3.6 [4]. It means that Dreft™ is 3.6 times more effective compared to Trifoam. This value was found by means of experiments on the air-water flow loop located at Delft University of Technology. No small scale test has been developed yet to find the scaling factor for other surfactants. Tab. 4.1 shows the effective and actual concentrations, as used in the present study. Note that Dreft™ is a mixture, consisting of surfactant and non-surfactant ingredients. The indicated concentrations consider the concentration of the entire mixture. The static surface tension was measured using a du Nouy ring tensiometer (Kr*ü*ss) at 20 °C. A platinum ring is raised through the air-water interface, and it thereby determines the force acting on the ring. The surface tension meter does not give a constant value, so the average of 3 measurements is given for each concentration in Tab. 4.1.

Table 4.1: Concentration values of Dreft™ used in the experiments and the corresponding static surface tension at 20 $°C$

Effective concentration (C_{eff}) [ppm]	Actual concentration (C) [ppm]	Static surface tension (γ) [mN/m]
0	0	76.5
500	139	73.7
1000	278	70.4
1500	417	67.4
3000	833	58.0

Before continuing with new experiments in the loop, a sample was taken from the loop by opening one of the drains. This sampled was taken to the lab to measure the surface tension. The value can be compared to the values in Tab. 4.1 to see whether the surface tension corresponds to a concentration of 0 ppm. If the flushing process is not done properly, the measurements of the next experiment will be affected by the left-over concentration of Dreft™ in the system.

Chapter 5

Results

This chapter discusses the results of experiments conducted in the Severe Slugging Loop. First, the reproducibility of the pressure measurements is discussed. The initial measurements were taken twice, over two consecutive days, to determine if the effectiveness of the surfactant reduces over time.
The first Sections discuss the effect of the surfactant on different types of slugging. Sec. 5.2 discusses the effect on slugging in the flowline. Sec. 5.3 discusses the effect on severe slugging. Sec. 5.4 discusses the effect on slugging in the riser. Sec. 5.5 discusses the effect of surfactants on the pressure gradient in the riser. These measurements were initially taken at a constant superficial liquid velocity and later at a constant gas-to-liquid ratio. Sec. 5.6 discusses the effect of surfactants on the developing length of the air-water mixture in the riser. The final section, which is Sec. 5.7, discusses the effect of surfactants on the liquid and foam collective holdup in the riser.

5.1. Reproducibility of pressure measurements

The first experimental run with surfactants was carried out twice to determine the reproducibility of the results and to understand if the surfactant deteriorates over 24 hours. The loop was run with u_{SG} = 1.21 m/s, u_{SL} = 0.40 m/s and an effective surfactant concentration of 500 ppm. The differential pressure on the flowline and the pressure drop in the riser were measured and later compared.

Fig. 5.1 shows the comparison of the pressure drop in the riser, measured in two consecutive days. A margin for the error should be taken into account, due to the finite accuracy of the pressure indicators. The pressure drop in the riser is calculated by subtracting the pressure at the top of the riser (PI-315) from the pressure at the bottom of the riser (PI-309). The error due to the pressure measurements should therefore be accounted for twice. The accuracy of a single pressure indicator is ± 0.2% for the full range of 10 bar. As this figure represents the average pressure drop per meter, i.e. Pa/m, this corresponds to 238 Pa/m. The error margin of 238 Pa/m is added to one of the measurements, indicated by the grey-shaded area. The other measurement (taken on another day) falls well within this boundary. The measurements show a small phase shift for a few points in the figure, e.g. between 45-47 s. However, over the full range of 600 s, both measurements have the same periodicity. The zoomed Fig. 5.1b also shows that the measurement of one day falls within the error margin of the measurement of another day. The differences between the measurements can be considered to be non-significant .

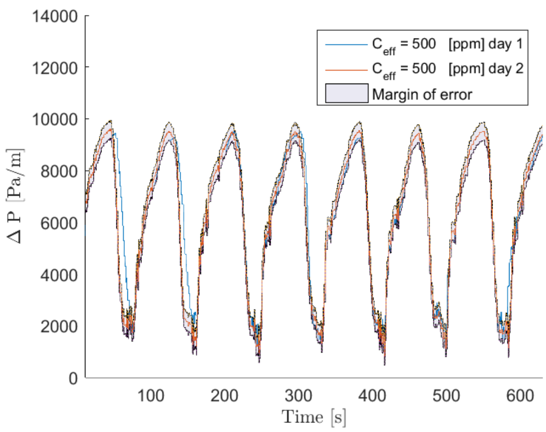

(a) Full range

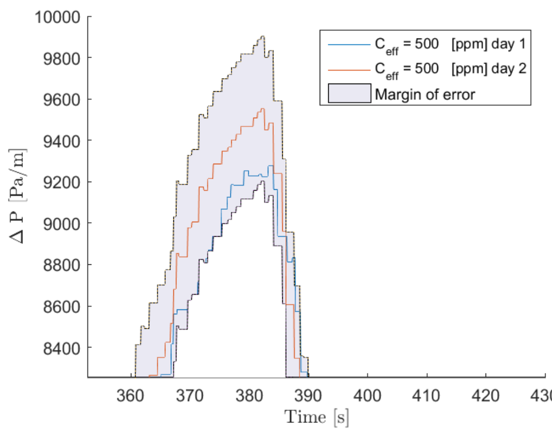

(b) Zoom

Figure 5.1: Comparison of the riser pressure drop with an effective surfactant concentration of 500 ppm. The measurements were taken on two consecutive days with u_{SG} = 1.21 m/s and u_{SL} = 0.40 m/s. The grey-shaded area shows an error margin of 5%.

Fig. 5.2 compares the differential pressure at two locations along the flowline. Fig. 5.2a represents DPI-430, located 10.5 m from the air injection point on the flowline. Fig. 5.2b represents DPI-120, located 46.7 m from the air injection point on the flowline, 0.2 m upstream of the bend. The DPIs have an accuracy of 2.2% over the full range of 100 mbar. As the differential pressure is measured over 3 m, this corresponds to 0.73 mbar/m. The measurements do not show any significant differences in terms of periodicity nor for the amplitude.

Fig. 5.1-5.2 show similar results for both days on which the measurements were taken. One can conclude that the surfactant does not change in "effectiveness" over 24 hours.

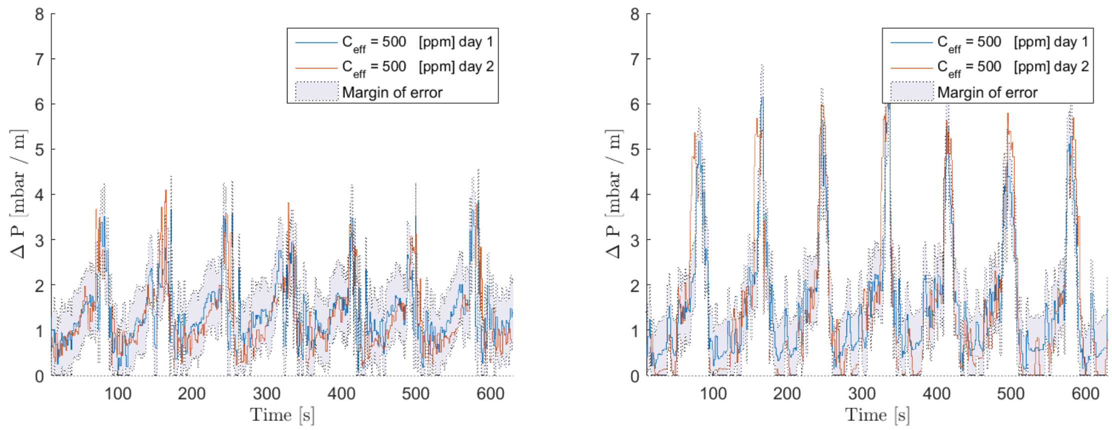

(a) DPI-430

(b) DPI-102

Figure 5.2: Comparison of differential pressure for two DPIs on the flowline. The effective surfactant concentration is 500 ppm. The measurements were taken in two consecutive days with u_{SG} = 1.21 m/s and u_{SL} = 0.40 m/s.

5.2. The effect of surfactants on slugging in the flowline

When operating the SSL in configuration # 1 with a superficial gas and liquid velocity u_{SG} = 1.21 m/s and u_{SL} = 0.40 m/s, slugging in the flowline is observed. Through the inspection glass on the flowline, it was observed that the slugs can be identified as growing slugs. These are relatively long slugs, with a length of up to 1200 pipe diameters (± 450 m) in a flowline of a full scale production system. The slug is initiated due to a growing instability of the air-water interface in the stratified flow regime. Once this instability grows, a slug is formed. After the slug passes, the flow stabilizes to the stratified flow again, which explains the relatively long length of the liquid slug.

By using the Distributed Acoustic Sensing (DAS), the slug units can be detected. Fig. 5.3 shows the signal-to-noise ratio (SNR) ψ as function of depth (i.e. length of the fiber) and time. As explained in Sec. 4.3.1, there are 9 beams visible. A single beam corresponds to 30 m of fiber length that is mounted onto the flowline. As the fiber is wrapped 9 times, the Frequency Band Extracted (FBE) data show 9 beams with a high SNR. The output is therefore mirrored for e.g. the first beam (top) and the second beam (top). In between these beams, indicated by the blue areas, the fiber is winded and not connected to the flowline. These parts of the fiber do not give a high SNR.

The fibers connected to the top of the flowline give the clearest FBE data. Due to gravity, the air flows on top of the water. When the liquid slug passes, the water will touch the top of the flowline wall. This movement is registered by the fiber connected to the top of the flowline and converted into an increase in the SNR. Six liquid slugs are clearly visible in the time frame, indicated by a high ψ value, i.e. the red areas.

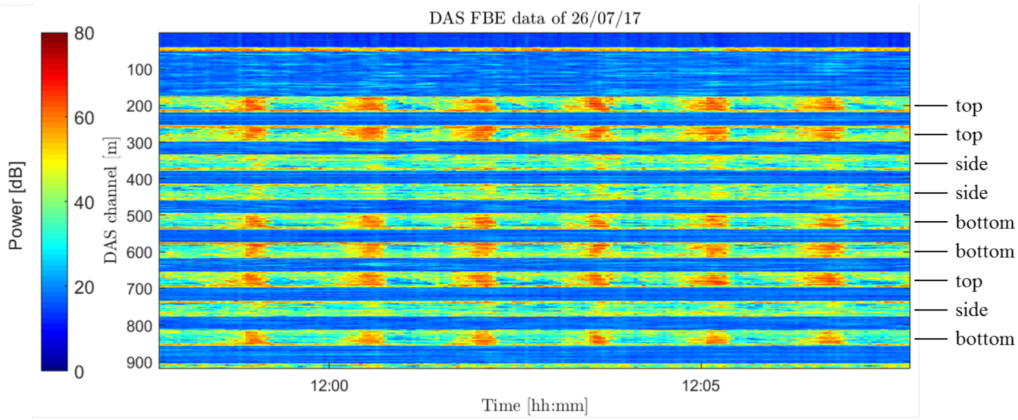

Figure 5.3: ψ as function of time and depth along the flowline.

For the characterization of the slug flow, the following steps are taken:

- **Slug time**: Fig. 5.4 shows the SNR ψ as function of time for channel #275. As explained in Sec. 4.3.1, a channel represents 1 m of fiber, mounted along the flowline. From the figure, one can determine the slug time (Δt_{slug}) and the slug frequency (f_{slug}). The average SNR (ψ_{avg}) forms a threshold, dividing the plot into two parts: 1) the (noisy) part exceeding the threshold, represented by the liquid body of the slug, and 2) the part below the threshold, represented by the gas bubble of the slug [14]. Note that for this analysis, it is assumed that slug flow consists of alternating pockets of liquid and gas. As seen in Fig. 5.3, six slugs are identified. The slug propagation time for each slug is given in Tab. 5.1. The average Δt_{slug} = 93 s. This corresponds to a slug frequency of 10.8 mHz.

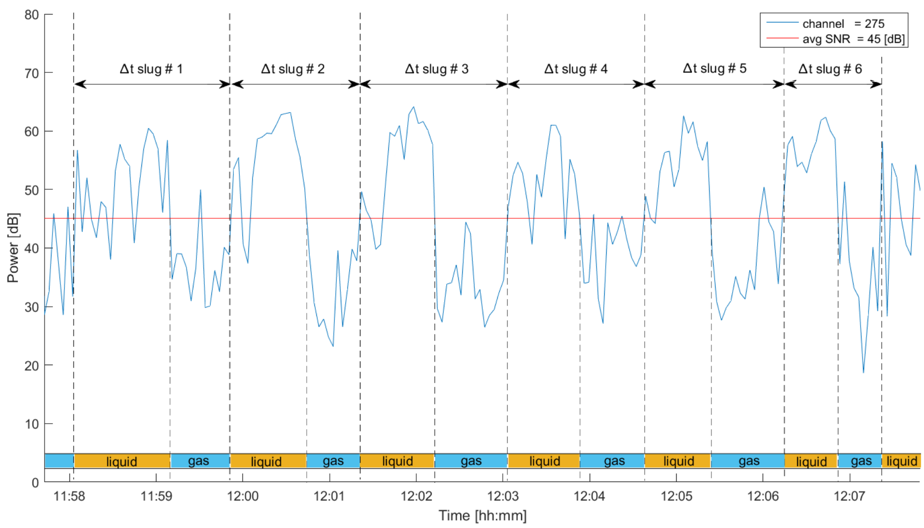

Figure 5.4: Slug identification for channel #275. The average SNR is added to the plot, in order to set a threshold. A slug unit consists of a noisy liquid pocket, and a more silent gas pocket.

- **Slug velocity**: There are two options to obtain the slug velocity (v_{slug}). The first option is to analyze the SNR as in Fig. 5.4. In Fig. 5.5, two SNRs are plotted for two channels: channel #263 and channel #293. The curves correspond to the SNR on two locations of the fiber, both located on top of the riser with a distance of 30 m between them. One can see a shift in the curves: this is the time during which the slug has travelled, from channel #263 to channel #293. As the distance that the slug has traveled is known, the velocity can be determined.

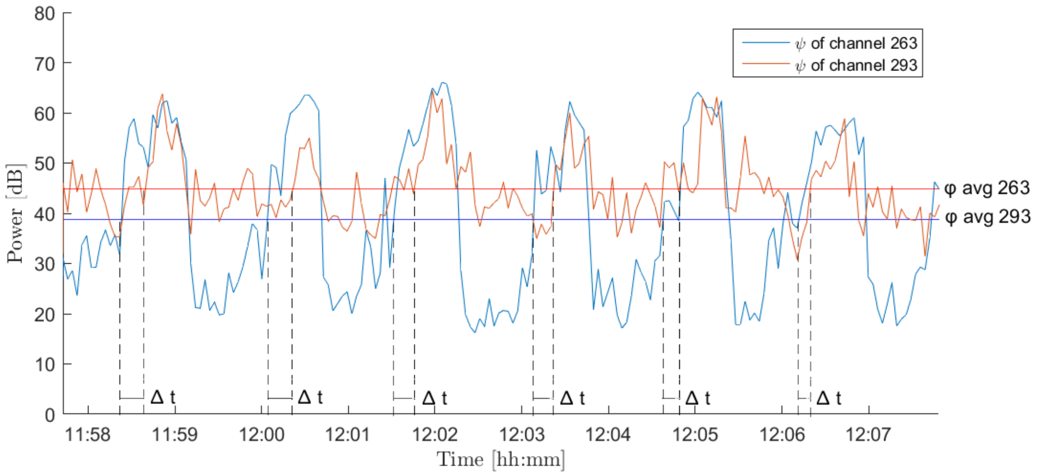

Figure 5.5: Slug travel time between channel #263 and channel #293. The average SNRs are added to the plot, in order to set a threshold for slug identification.

The second option to obtain the slug velocity is by means of the velocity tracking tool in the OptaSense DxS Browser software (Sec. 4.3.1). In App.E.1 a figure is shown of the velocity tracking tool interface. The software allows one to pick points in the figure. It automatically returns the slug velocity by assessing the slope between two points.
The velocity tracking tool is an intuitive way of determining the velocity, as the user can choose the location of the points. It was therefore chosen to use the SNR method. The calculated velocity is given in Tab. 5.1.

- **Slug length**: The slug time and slug velocity can be used to determine the slug length ($L_{slug} = v_{slug}\Delta t_{slug}$). The slug length consists of a liquid body and a gas bubble. The slug properties for each of the 6 slug units, as identified in Fig. 5.4, are given in Tab. 5.1.

Table 5.1: Slug properties for each of the 6 slug units as identified in Fig. 5.4

Slug #	Duration [s]			Length [m]			Velocity [m/s]
	Bulk	Liquid	Gas	Bulk	Liquid	Gas	
1	107	66	41	53	33	20	0.50
2	89	53	36	44	26	18	0.50
3	102	52	50	60	31	29	0.59
4	95	50	45	58	30	27	0.61
5	95	46	49	70	34	36	0.73
6	67	38	29	69	39	30	1.03
Average	93	51	42	59	32	27	0.66

Fig. 5.6 - Fig. 5.8 show the signal-to-noise ratio 1) as a function of time for channels #250-300, and 2) as function of time for channel # 275. Air-water is compared to a concentration of 500 ppm (Fig. 5.7) and 1000 ppm (Fig. 5.8). For air-water (C=0 ppm), the six slug units are clearly visible in the flowline. However, when adding the surfactant at concentrations of 500 ppm and 1000 ppm, the slugs disappear. For the air-water (C = 0 ppm) plot, a slug identification analysis can be done, as described earlier in this section. However, as there are no slugs when the surfactant is added to the mixture, characterization of the slug units is impossible. This indicates that flowline slugging is suppressed by the surfactant. Furthermore, the average SNR decreases for increasing surfactant concentration.

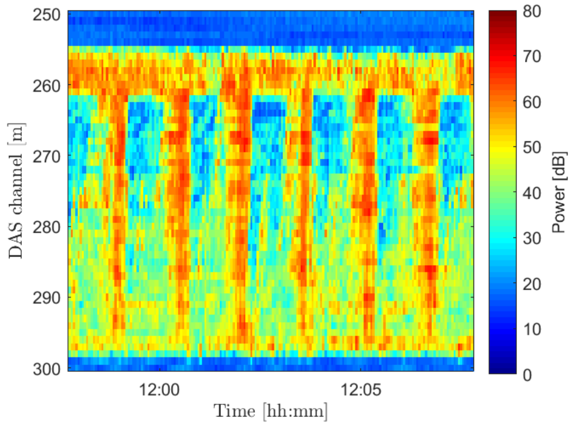

(a) ϕ as function of time and depth

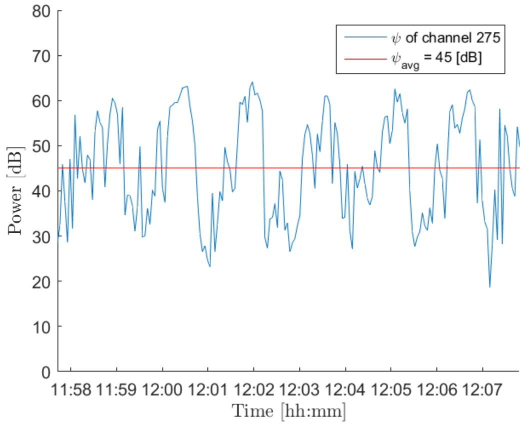

(b) ϕ as function of time

Figure 5.6: C_{eff} = 0 ppm

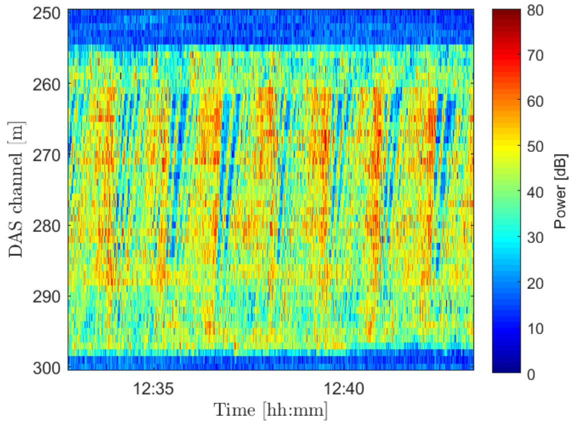

(a) ϕ as function of time and depth

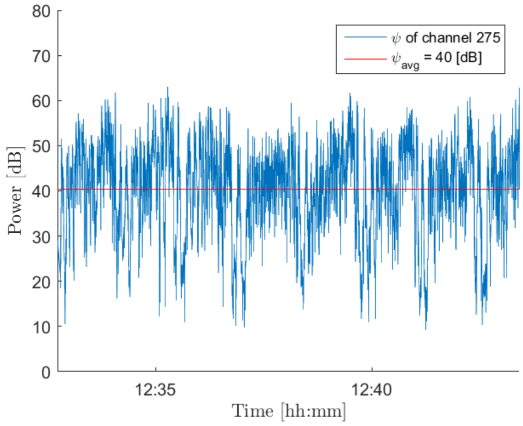

(b) ϕ as function of time

Figure 5.7: C_{eff} = 500 ppm

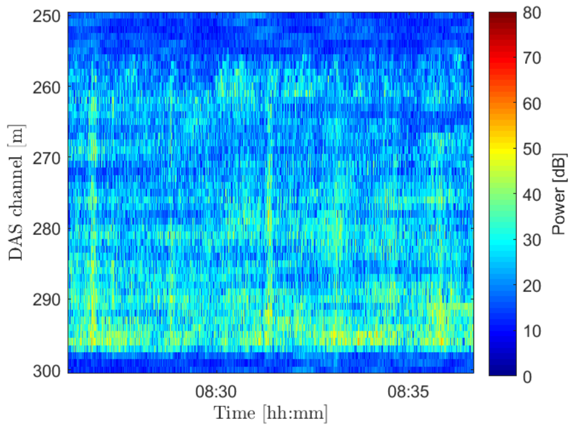

(a) ϕ as function of time and depth

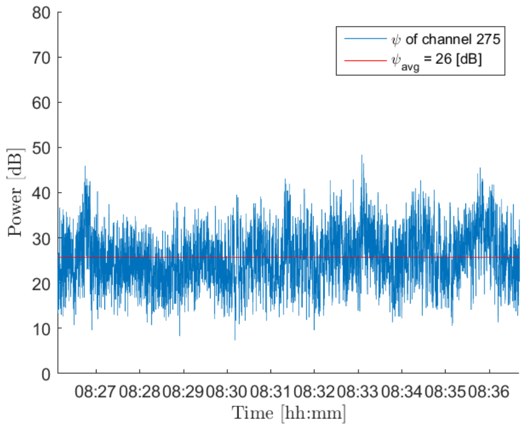

(b) ϕ as function of time

Figure 5.8: C_{eff} = 1000 ppm

The effect of the surfactant on slugging in the flowline is also detectable from the pressure measurements. Fig. 5.9 shows the pressure measurements for effective concentrations of 0 ppm, 500 ppm and 1000 ppm. The Figure on the left (Fig. 5.9a) shows the differential pressure over the riser. The figure on the right (Fig. 5.9b) shows the differential pressure of DPI-102 on the flowline. By adding the surfactant to the air-water mixture, the cyclic behavior of flowline slugging is suppressed. The pressure build-ups disappear with surfactants. For C_{eff}= 1000 ppm, the differential pressure along the riser levels off to a value of 4000 Pa/m.

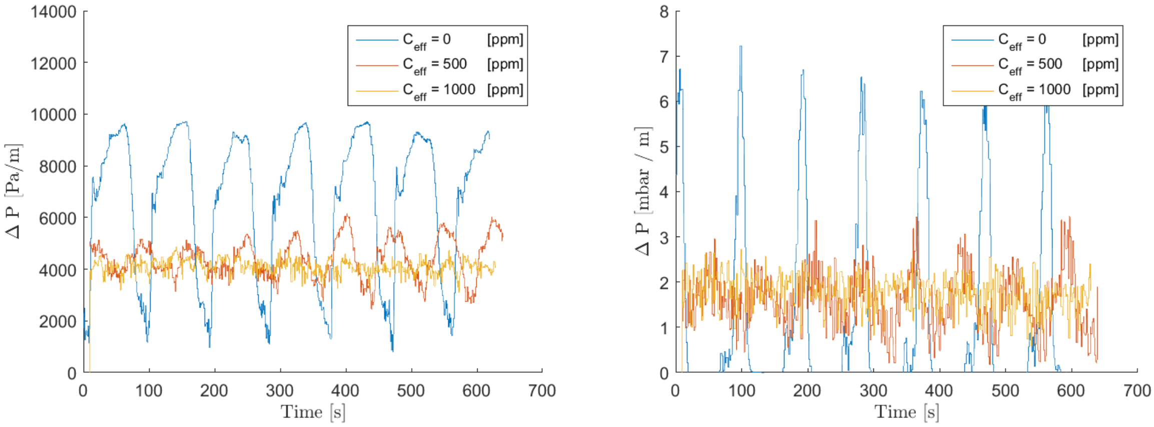

(a) Differential pressure over the riser

(b) Differential pressure (DPI-102)

Figure 5.9: Pressure measurements for multiple effective surfactant concentrations and with u_{SG} = 1.21 m/s and u_{SL} = 0.40 m/s.

5.3. The effect of surfactants on severe slugging

This Section discusses the effect of surfactants on severe slugging. Severe slugging occurs in flowline riser systems, so configuration #1 was used for this analysis.

Fig. 5.10 shows the pressure drop along the riser during a severe slugging cycle. For the air-water (C = 0 ppm) mixture, a pure slugging cycle is visible; it has a regular oscillatory behavior. The pressure build-up of 1.6 bar corresponds to a full water column in the riser of 16.8 m. When the surfactant is added in a sufficiently high concentration (C > 1500 ppm), this regular oscillatory behavior changes. Fig. 5.10a shows the riser pressure drop with an effective surfactant concentration of 1500 ppm. The severe slugging cycle is still visible. The maximum pressure build-up, however, is not reached continuously anymore. There is a shift in type of severe slugging, as indicated by R. Malekzadeh (2012) [15]. The severe slugging cycle for the air-water case is considered a type 1 severe slugging cycle. The liquid body of the slug fills up the total riser length. However, when surfactants are added, a severe slugging cycle of type 2 is noticed. This type 2 cycle is qualitatively similar to a type 1 cycle, thought the slug length is shorter than the riser height. The liquid at the riser base is penetrated by the gas before it has filled the full riser length. This phenomenon gives intermittent unstable oscillations, as marked by the irregular pressure drop cycle. The shorter slugs appear more frequently. The frequency of the pressure build-up increases from 9.2 mHz for air-water to 10.4 mHz for a concentration of 1500 ppm.

Fig. 5.10b shows the riser pressure drop with an effective surfactant concentration of 3000 ppm. At this concentration, there are no slugs that fill up the whole riser length. An increase in the concentration of the surfactant leads to a decrease in the slug length. The frequency has increased again, to a value of 11.3 mHz. In the plots it can be seen that surfactants do not prevent the severe slugging cycle. However, surfactants lead to a disruption of the continuous pressure build-up. The maximum pressure is reached less often at the riser base. It can therefore decrease fatigue on the tubing at the riser base.

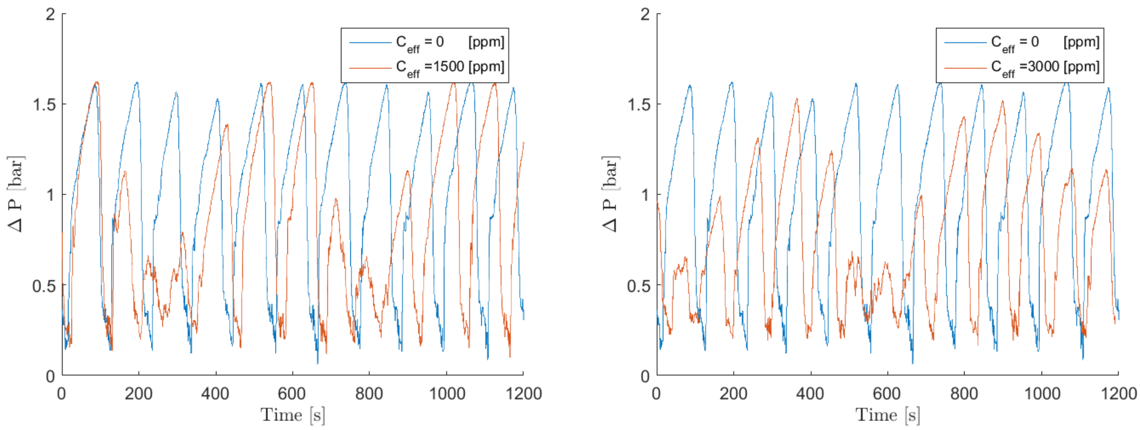

(a) C_{eff} = 1500 ppm

(b) C_{eff} = 3000 ppm

Figure 5.10: Riser pressure drop for a severe slugging cycle with u_{SG} = 1.42 m/s and u_{SL} = 0.27 m/s.

5.4. The effect of surfactants on slugging in the riser

For the analysis of the effect of surfactants on slugging in the riser, configuration #2 of the SSL is used. The multiphase flow in the riser of the SSL is in the slugging regime, when operated at u_{SG} = 0.37 m/s and u_{SL} = 0.27 m/s. Fig 5.11 shows the differential pressure over time measured at two locations in the riser. Fig. 5.11a shows the measurements for DPI-300 at the riser base, whereas Fig. 5.11b shows the measurements for DPI-302 at the top of the riser. Fig. 5.12 also shows the differential pressure over time for the concentrations of 500 and 1500 ppm. All figures show the same trend: an increasing surfactant concentration decreases the differential pressure. However, there is a slight difference in the measurements for the concentration of 1500 ppm. At the beginning of the plot (T = 0 - 90 s), the pressure gradient is relatively high. This is a result of a measurement error. It takes time for a multiphase flow to stabilize. In this case, the air-water mixture was was not stable yet, which is indicated by a decrease in differential pressure over time. The differential pressure measurements of DPI-301 are given in App. G. The comparison of all surfactant concentrations in one plot is also given in this Appendix.

Tab. 5.2 summerizes the findings of Fig. 5.11 and Fig. 5.12. The table shows the decrease in differential pressures in percentages compared to air-water, when a surfactant is added to the air-water mixture. At the bottom of the riser, the differential pressure decreases by 5.1% when an effective surfactant concentration of 3000 ppm is used. However, the effect is most pronounced for fully developed flow, which occurs at the top of the riser. At the top of the riser, the differential pressure decreases by 18.9% when an effective surfactant concentration of 3000 ppm is used.

Table 5.2: Decrease in the measured differential pressure with surfactants compared to air-water without surfactants; considered are multiple concentrations for three DPIs installed along the riser of the SSL.

C_{eff} [ppm]	DPI-300 [Δ%]	DPI301 [Δ%]	DPI302 [Δ%]
0	NA	NA	NA
500	-3.9	-14.2	-14.2
1000	-3.9	-14.6	-14.6
1500	-4.7	-15.7	-15.8
3000	-5.1	-18.7	-18.9

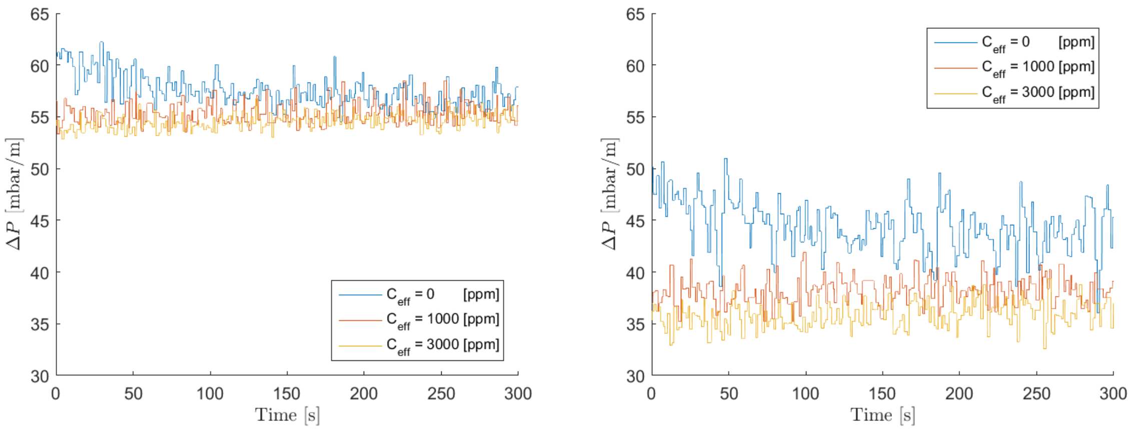

(a) DPI-300 (riser base) (b) DPI-302 (top of riser)

Figure 5.11: Comparison of differential pressure measured on two location on the riser of the SSL. Measurements were taken at u_{SG} = 0.37 m/s and u_{SL} = 0.71 m/s. Surfactant concentrations of 1000 and 3000 ppm are included.

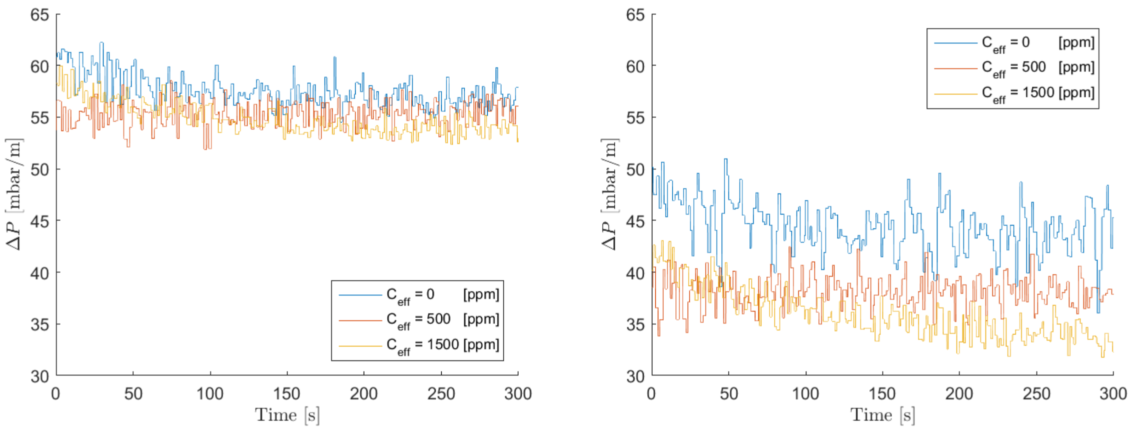

(a) DPI-300 (riser base) (b) DPI-302 (top of riser)

Figure 5.12: Comparison of differential pressure measured on two location on the riser of the SSL. Measurements were taken at u_{SG} = 0.37 m/s and u_{SL} = 0.27 m/s. Surfactant concentrations of 500 and 1500 ppm are included.

For an empty riser, i.e. a riser filled with air only, the DPIs should return a value of 0 mbar. However in practice this value fluctuates: the returned value is often between the 0 and 10 mbar. The starting value of each DPI was therefore marked for each run. When analyzing the data, this value was subtracted from the total output value over the range of 300 s.

The differences in the measured differential pressure are relatively small, especially for the DPI at the bottom of the riser (Fig. 5.11a and Fig. 5.12a). It is therefore important to take the accuracy of the DPI into account. The accuracy of the DPIs is ± 0.05% over the full range of 500 mbar. This corresponds to ± 0.08 mbar/m. This value is smaller than the differences in the measured differential pressure, as indicated in Tab. 5.2. The statement that surfactants decrease the differential pressure is therefore still valid.

5.5. The effect of surfactants on the pressure gradient

In order to find the effect of the surfactant on the pressure gradient, the Tubing Performance Curve can be considered for air-water flows with different concentrations. The pressure gradient in the riser is measured for a range of superficial gas velocities, with a constant superficial liquid velocity of 0.05 m/s. Fig 5.13 shows the TPCs for multiple surfactant concentrations. Configuration #1 is used here, in which both water and air are injected into the flowline.

At low gas flow rates, the pressure gradient is reduced when surfactants are added to the air-water mixture. A concentration of 500 ppm creates sufficient foam to suppress churning of the liquid film. The interfacial friction decreases and as a result also the pressure gradient decreases. However, when the surfactant concentration increases, more foam is created. This leads to an increase of the pressure gradient, as is seen for high gas flow rates.

At high gas flow rates, the pressure gradient is increased with increasing surfactant concentration. With high surfactant concentrations, a large amount of foam is created. It reduces the cross sectional area of the pipe. Due to the foam, the interfacial roughness increases, which leads to larger interfacial stress and hence a high pressure gradient. This effect is also visible in Fig. 5.13: 1) the minimum pressure gradient increases for increasing surfactant concentration, and 2) the minimum pressure point tends to shift towards low gas flow rates.

The above described findings confirm the findings by Van Nimwegen (2015) [1]. Van Nimwegen used a 50 mm diameter flow loop and a different water flow velocity, which explains the differences in the pressure gradient for air-water in this work. The measurements by Van Nimwegen were taken at a constant u_{SL} of 0.01 m/s. App.I shows the findings, considering multiple surfactant concentrations.

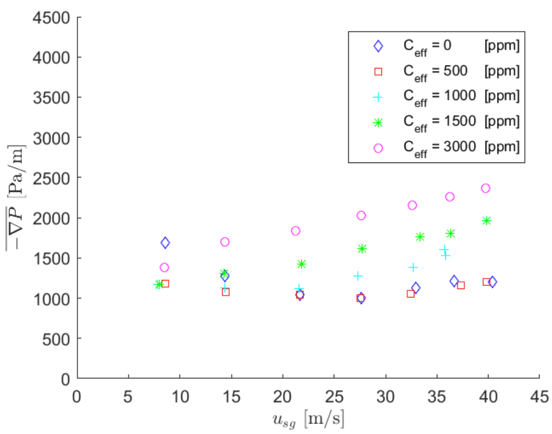

Figure 5.13: Comparison of TPCs for different effective concentrations of surfactant. Measurements were taken with u_{sl} = 0.05 m/s.

In the production of oil and gas, wells usually operate at a constant gas-to-liquid ratio, instead of at constant u_{SL}. The measurements in the second experiment were therefore taken at a constant GLR. With the limitations of the water pump and the mass flow controllers taken into account, the pressure gradient was calculated for GLR = 60 and GLR = 100. Fig. 5.14 shows the TPC for multiple surfactant concentrations, at constant GLR. Configuration #2 is used, in which air is injected into the riser, and water into the flowline. Fig. 5.14a shows that the pressure gradient is suppressed in the low gas flow rate region by the surfactant. The TPC becomes a straight line: the gravity dominated part diminishes, where high pressure gradients normally occur due to churning of the liquid film. For the concentration of 1500 ppm, there is one outlying measurement. Due to a communication failure of one of the pressure sensors, the pressure gradient has a significant high pressure gradient. Fig. 5.14b shows the TPCs for a constant GLR of 100. The figure is similar to the TPCs with a constant GLR of 60.

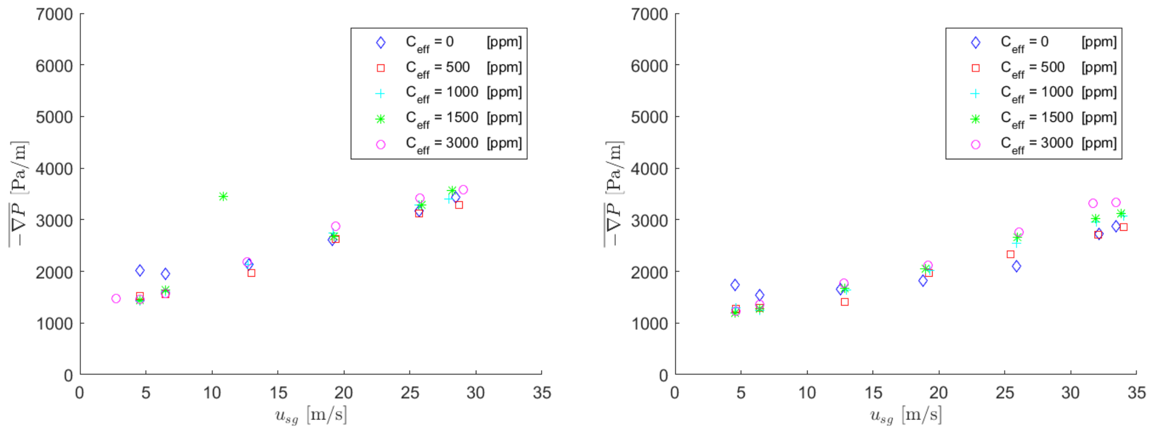

(a) GLR = 60 (b) GLR = 100

Figure 5.14: Comparison of TPCs for different surfactant concentrations in air-water. Measurements were taken at constant gas-to-liquid ratios.

5.6. The effect of surfactants on the developing length

To analyze the effect of the surfactant on the developing length, differential pressure measurements were taken on three locations along the riser. Configuration #2 of the Severe Slugging Loop is used for this analysis. As described in Sec. 4.1, the three locations are:

- DPI-300 at a height of 3.2 m on the riser, i.e. at the riser base
- DPI-301 at a height of 11.8 m on the riser, i.e. just below the top of the riser
- DPI-302 at a height of 15.0 m on the riser, i.e. at the top of the riser

Fig. 5.15 shows the pressure gradient measured at the riser base and at the top of the riser. Both air-water and air-water with a surfactant concentration of 3000 ppm are shown for GLR = 60 and GLR = 100. The air-water measurements are not identical, as the flow is still undeveloped at the riser base. When adding the surfactant, the measurement variation increases; the pressure gradient has decreased significantly at the top of the riser.

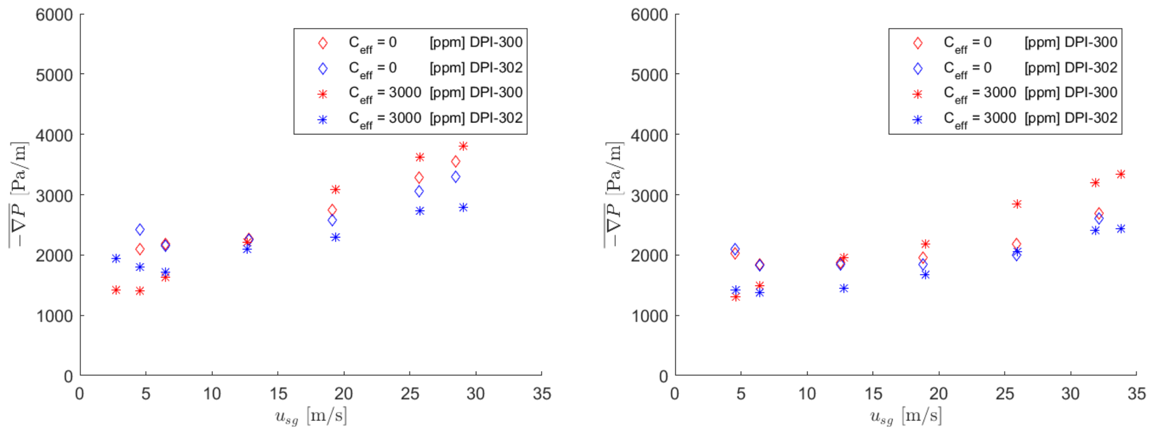

(a) GLR = 60 (b) GLR = 100

Figure 5.15: Differential pressure measured on two location on the riser of the SSL. DPI-300 is installed at the riser base, DPI-302 is installed at the top of the riser. See also Fig. 4.3 for the locations of the DPIs.

To find any effects on the developing length, one has to compare the DPIs that are located at a point at which the air-water flow is expected to be fully developed. Fig. 5.16 shows the TPCs measured by DPI-301 and

DPI-302, with GLR = 60. For an air-water (C = 0 ppm) mixture, the measured pressure gradient measurements are approximately equal for both locations on the riser top. For a concentration of 1000 ppm added to the air-water mixture, this still holds. However, when the concentration is increased to 3000 ppm, the measurements show differences. The pressure gradient measurements begin to vary more between the two locations, especially at high air flow rates. This is an indication that 1) the flow has not fully developed yet at the top of the riser, and that 2) the developing length increases when the surfactant is added in this concentration. Fig. 5.17 also shows the TPCs measured by DPI-301 and DPI-302, though with a GLR = 100. The pressure gradient measurements show a larger spread for the two measurement locations on the riser, indicating that the effect is more pronounced for high gas-to-liquid ratios.

Van Nimwegen (2015) [1] has also analyzed the effect of surfactants on the flow development in a 50 mm riser. The findings are given in App. J. Measurements were taken at a constant u_{SL} = 0.01 m/s and a concentration of 1000 ppm. In his study, a concentration of 1000 ppm increases the developments length. A 1-1 comparison cannot be made as Fig. 5.15 - Fig. 5.17 were taken at a constant GLR, instead of at a constant u_{SL}. For a GLR=60, this corresponds to a u_{SL} range of 0.05-0.34 m/s, and for a GLR=100, this corresponds to a u_{SL} range of 0.05-0.48 . Hence, this study makes use of larger liquid flow rates. As a results, the effect of the surfactant only becomes detectable when using a concentration of 3000 ppm: the surfactant increases the development length. The study therefore confirms the findings by Van Nimwegen.

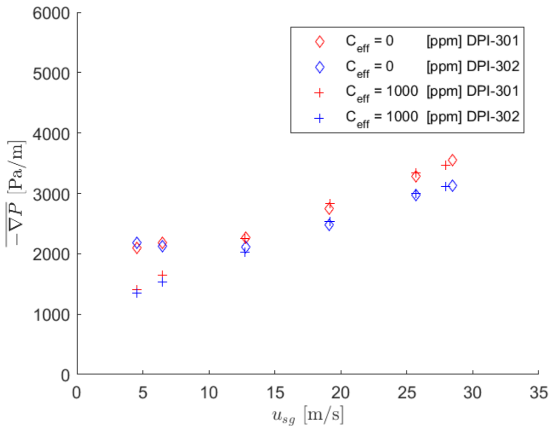

(a) C_{eff} = 0 and C_{eff} = 1000 ppm

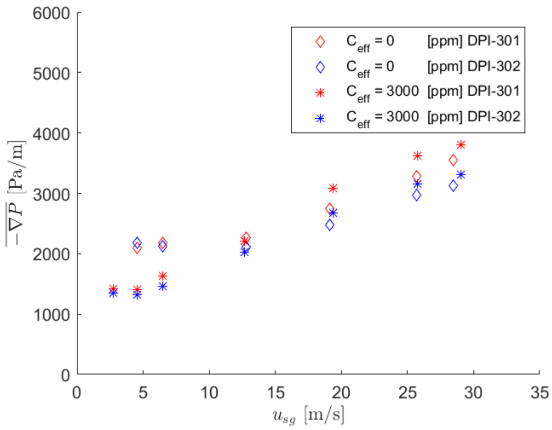

(b) C_{eff} = 0 and C_{eff} = 3000 ppm

Figure 5.16: Differential pressure measured on two location on the riser of the SSL. The gas-to-liquid ratio is equal to 60.

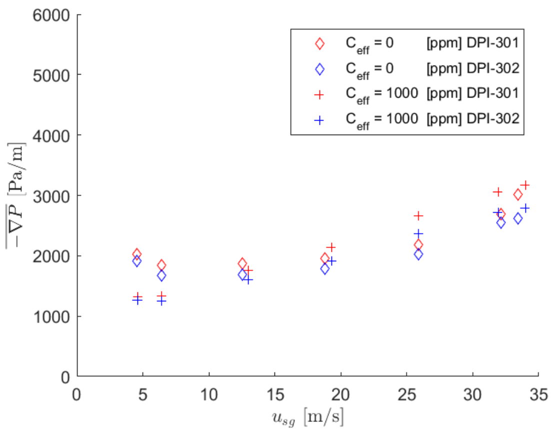

(a) C_{eff} = 0 and C_{eff}= 1000 ppm

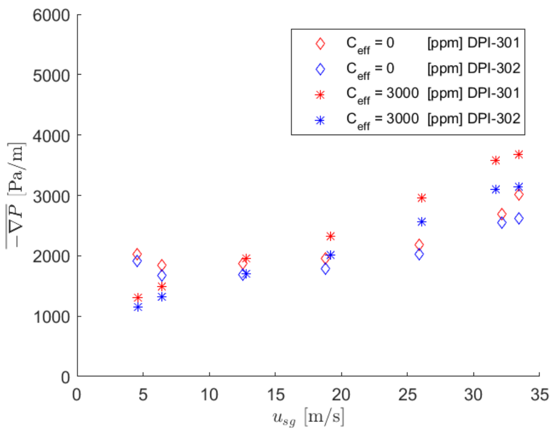

(b) C_{eff} = 0 and C_{eff}= 3000 ppm

Figure 5.17: Differential pressure measured on two location on the riser of the SSL. The gas-to-liquid ratio is equal to 100.

5.7. The effect of surfactants on the holdup fraction

This section discusses the effect of surfactants on the holdup fractions. Two holdups are considered: the liquid holdup and the foam holdup. The liquid holdup (α_l) is the cross sectional area of the liquid phase divided by the total area, as given in Eq. 2.12. The foam holdup (α_{foam}) is the cross sectional area of the liquid and the foam, divided by the total area. To calculate the foam holdup, the Shell Flow Correlations make a distinction between the liquid layer height (δ_l) and the foam layer height (δ_f), as given in Eq. 3.1. The foam layer has a gas content (c_g) and a liquid content (c_l). The total height of the liquid is given by:

$$\delta_{total-liquid} = \delta_l + c_l \cdot \delta_f \tag{5.1}$$

When operating the Severe Slugging Loop with air-water and a surfactant, the liquid layer is located along the pipe wall. The foam layer is located between the liquid layer and the gas core, as is shown in Fig. 3.5. As soon as the quick closing valves are shut by the operator, the liquid layer and foam layer fall down into the piece of piping in between both valves. This is shown on the left in Fig. 5.18. At the moment directly after closing the valves, the liquid layer and foam layer are still mixed; no distinction can be made between both layers. However, after some time (± an hour), gravity will force the liquid to separate from the foam and to fall down. This is shown on the right in Fig 5.18. At this point, the different layers are becoming visible: a liquid layer on the bottom, covered by a layer of foam. The gas is located on top of these layers. One could wait some hours longer, for the foam to collapse. The liquid in the column would give the total liquid holdup, as in Eq. 5.1.

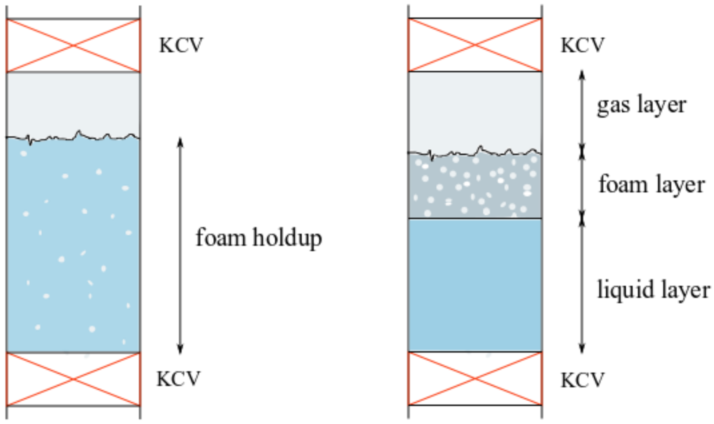

Figure 5.18: The two situations after closing the quick closing valves on the riser. Directly after the valves are closed (left), the foam and liquid are still mixed. After ± an hour (right), the liquid falls down and is covered by a layer of foam.

A scale was connected to the riser, to measure the height of the foam, i.e. the foam holdup as shown in Fig. 5.18. Note that the measurement was taken directly after simultaneously closing the quick closing valves, so the liquid and foam were still mixed. Due to a constraint in time, it was decided not to wait for the liquid to fall down such that the three different layers became visible. Also, it was decided not to wait for the foam to collapse entirely, to calculate the total liquid holdup. The latter would require several hours for each measurement.

Fig. 5.19 shows the results of simulations, which were done by calling a .dll file of the Shell Flow Correlations in MATLAB. The plots are made for a constant GLR of 60, and for multiple surfactant concentrations. Fig. 5.19a shows the liquid holdup and Fig. 5.19b shows the foam holdup. For increasing surfactant concentration, two trends are noticeable: 1) the liquid holdup decreases, and 2) the foam holdup increases.

The liquid holdup is a function of the height of the liquid layer along the pipeline and the liquid content of the foam which is created by the surfactant. For an increasing surfactant concentration, both the liquid layer and the liquid content of the foam decrease. This results in an overall decrease in liquid holdup. At u_{SG} > 30 m/s, the liquid holdup levels off: it becomes independent of the surfactant concentration and the gas flow rate.

For high surfactant concentrations, a larger amount of foam can be created. This explains the increase in foam holdup for high concentrations in Fig. 5.19. For small gas flow rates, i.e. $u_{SG} < 6$ m/s , the foam holdup shows the same behavior as the liquid holdup: it decreases with increasing surfactant concentration. For larger gas flow rates, i.e. $u_{SG}>6$ m/s, this behavior changes. The high gas flow rates stimulate the creation of foam for high surfactant concentrations. However, the overall foam holdup decreases for increasing gas flow rates. Constant GLRs are considered, so when the gas flow rate increases, the water flow rate increases at the same rate. From the experiments, one could see that the structure of the foam depends on these gas flow rates. Air was vented to the atmosphere from the separator. At high concentrations, large amounts of foam were created. Some foam was vented to the atmosphere (with the air), and eventually landed on the ground. Clearly, the structure of the foam was different for each run: it was either dry and hard to break down, or wet and easy to break down (e.g. by adding some water). It was found that at large water and gas flow rates, a wetter and denser foam was created, containing small air bubbles. This confirms the flow visualization findings by Van Nimwegen (2015): pipe flows with surfactants show more large bubbles at small liquid flow rates. In other words, the gas content is smaller at large air and water flow rates. This results in a decreasing foam holdup for increasing flow rates, as shown in Fig. 5.19. At high air flow rates, i.e. $u_{SG} > 40$ m/s, the foam holdup levels off: it becomes independent of flow rates and surfactant concentration.

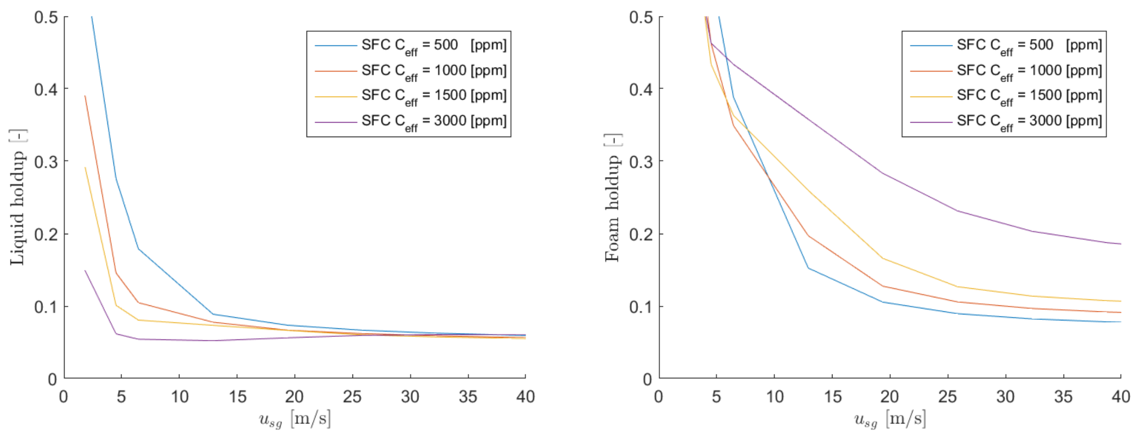

(a) Liquid holdup (b) Foam holdup

Figure 5.19: Comparison of liquid and foam holdup simulation results with the Shell Flow Correlations (SFC) for GLR = 60.

Fig. 5.20 and Fig. 5.21 show the foam holdup results. The experimental results are compared with the simulation results from the Shell Flow Correlations for both GLR = 60 and GLR = 100. The experimental holdup measurements show a spread. This might be due to the transient behavior of the flow. For low gas flow rates, i.e. in the slugging regime, the flow has an unsteady behavior. For high gas flow rates, e.g. in the annular foam regime, the flow behavior is more steady, though it also shows some transients. On average it is assumed that the behavior of the flow is steady, though the transients in the flow affect the foam holdup measurements. The measurements depend on the precise moment of closure of the valves. In the case of slug flow, it could be the liquid slug body or the gas bubble of the slug that is shut in by the quick closing valves. It would therefore be instructive to perform several foam holdup measurements and determine the average and standard deviation.

The four plots show the same effect for small gas flow rates: the simulations over-predict the foam holdup. This confirms the findings by Van Nimwegen (2015). The measurements in the low gas flow rate region are below the flow rate for the churn-annular transition. In the riser, this means that the film moves up and down intermittently. However, the model predicts liquid down-flow near the wall, resulting in a significant negative frictional pressure gradient [4]. For a constant total pressure gradient, this results in a high hydrostatic pressure gradient. The latter is a function of the holdup, hence the holdup is overestimated by the model.

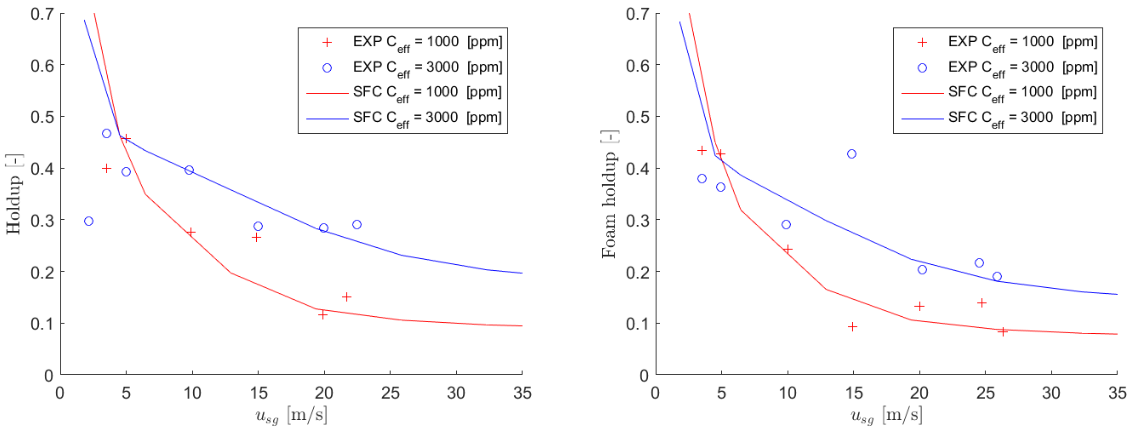

(a) GLR = 60 (b) GLR = 100

Figure 5.20: Comparison of foam holdup results for multiple surfactant concentrations. Experimental results are shown by the symbols. SFC simulation results are shown by the lines.

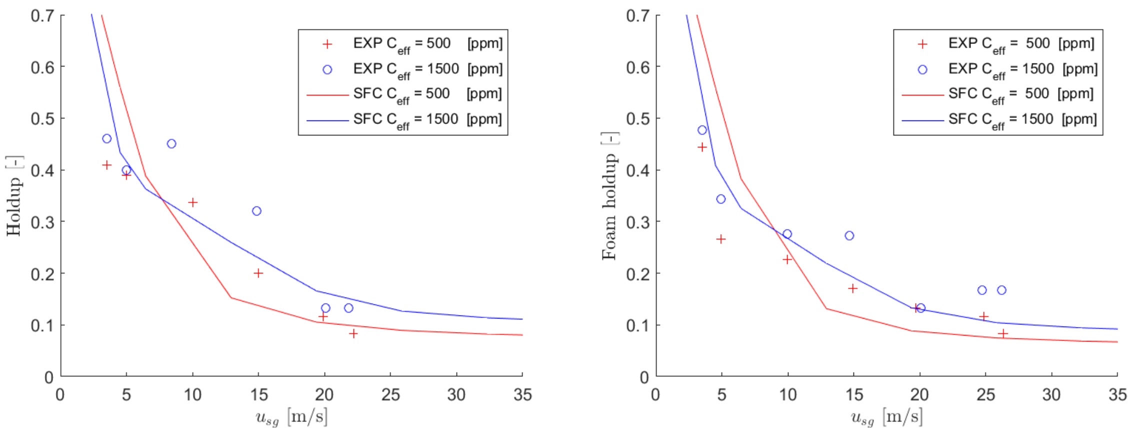

(a) GLR = 60 (b) GLR = 100

Figure 5.21: Comparison of foam holdup results for multiple surfactant concentrations. Experimental results are shown by the symbols. SFC simulation results are shown by the lines.

Chapter 6

Conclusions

Due to the success of the application of surfactants in vertical wells, it is of interest to investigate whether surfactants can also help to overcome liquid management problems in surface flowline-riser systems. The objective of this work was therefore to find the effect of surfactants on two-phase air-water mixtures in flowlines and risers.

Experiments were carried out in the Severe Slugging Loop at the Shell Research and Technology Centre Amsterdam. The flow loop consists of a 100 m horizontal and downward inclined flowline with an inner diameter of 0.051 m, and a 16.8 m vertical riser with an inner diameter of 0.044 m. The working fluids are air and water, and operation is at atmospheric outlet pressure. The dish washing detergent Dreft ™ was used in multiple concentrations to create foam. Various measurement techniques were used: (Differential) Pressure Indicators (DPIs and PIs), Distributed Acoustic Sensors (DAS), quick closing valves and flow visualization.

The following conclusions can be drawn with respect to the effect of surfactants on two-phase flows in flowlines and risers:

- Growing slugs in the flowline can be mitigated by adding a surfactant to the air-water mixture. The slugs fully disappear when an effective surfactant concentration of 1000 ppm is added.
- The severe slugging cycle in a flowline-riser system is not prevented when a surfactant is added. The measured pressure drop over the riser height does change: the liquid slug build-up becomes irregular. This is because a significant amount of gas, which is present in the foam, enters the riser. An effective concentration of 3000 ppm shows a slight decrease in the severe slugging cycle period.
- Slugging in the riser cannot be mitigated by adding a surfactant to the air-water mixture. However, the differential pressure along the riser is decreased, due to the creation of foam. For a concentration of 3000 ppm, the differential pressure reduces by 5.1% at the riser base and by 18.9% at the top of the riser.
- The development length of air-water in a vertical riser is slightly increased when surfactants are added. The effect is visible when a concentration of 3000 ppm was used, for a gas-to-liquid ratio of 100. The differential pressure measurements taken at two locations at the top of the riser showed differences. This is an indication that the air-water mixture has not fully developed yet.
- For low gas flow rates, surfactants decrease both the liquid and foam holdup. For high gas flow rates, the behavior for the foam holdup changes. Two observations can be made from the experimental results and the simulation results with the Shell Flow Correlations. First, surfactants increase the foam holdup, due to a larger amount of foam that can be created with larger concentrations. Second, the foam holdup decreases with increasing gas and water flow rates. This is due to a change in foam structure: large flowrates create a foam with small bubbles, which results in a lower foam holdup.

Chapter 7

Recommendations

Recommendations with respect to the experimental setup

- The surfactant was introduced to the flowloop by pre-mixing it with water in the large water vessel (V-104) on the ground. The mixing was done by stirring the water containing the surfactant manually with a stick. It can lead to an irregular distribution of the surfactant in the vessel. Eventually during start up, the pump will introduce water into the system, which might not contain the exact right concentration of the surfactant. To ensure a uniform distribution of the surfactant, a mixing machine could be used.

- Two configurations of the Severe Slugging Loop were used in this work. For each configuration, a set of experiments was conducted in which the concentration of the surfactant was increased. For the second set of experiments, extensive flushing of the loop was required to remove all surfactant remainders from the system. The loop was first drained entirely, and flushed with air to get all water out. This was followed with flushing the loop with water. However, flushing might not be enough to remove all surfactant particles. It is recommended to not only flush, but also clean the system thoroughly. This includes decommissioning and extensive cleaning of the inside of the tubing and vessels. Special attention should be given to the separator and the vessel above, as the foam sticks to the walls on the inside, where it is inaccessible.

- The operator of the SSL can set a certain gas flow rate when conducting experiments. The gas flow rate is independent of the system pressure. In the production of oil and gas, the gas flow rate is not constant. The gas flow rate is determined by the pressure drop between the reservoir pressure and the pressure at the bottom hole of the well. A feedback loop could be made for the SSL, which takes the pressure at the bottom of the riser (PI-309) into account. In this way, the gas flow rate is dependent on the system pressure instead of having a fixed value.

- At effective surfactant concentrations of 1500 ppm and larger, the foam started to leave the separator together with the air at the top of the setup. It is recommended to connect a flexible hose to the tubing where air is vented to the atmosphere. If the hose is long enough (i.e. larger than 16.8 m), the foam can be collected at the ground. It will also prevent the foam from flying around in case of winds, making the stairs of the setup and the ground around the setup slippery.

- Experimental foam holdup measurements have shown a wide spread. The reason for this is the transient behavior of the flow in the riser. It is recommended to do multiple measurements next time for each experimental run, after which the average and standard deviation of the foam holdup is calculated.

Recommendations for further research

- The small-scale experiments as conducted in this work are a proof of concept. It is recommended to do a scale-up of the experiment, to get a better understanding of the effect of surfactants in oil and gas production systems. A scale-up would include a large diameter, high pressures, high temperatures, the use of another surfactant and potentially the addition of oil into the system.

- A film-model has been incorporated in the Shell Flow Correlations, making it possible to validate the experimental results with simulations. However, this model is able to compute multiphase flow characteristics for upward vertical and inclined flows only. No model has been developed yet to compute the characteristics of horizontal multiphase flows with foam. The model for horizontal flows differs from the vertical flow model, as horizontal flows are not axi-symmetric.

- The acoustic fibers of the DAS apparatus were installed along the flowline. It is recommended to install DAS fibers along the riser as well. The DAS data can give a better insight by visualizing the effect of surfactants on slugging in the riser.
- A recent field trial with foam injection into a well in Gabon has shown that the foam, which by accident had entered the flowline, reduced the pressure gradient in the flowline. Higher production rates where achieved. It is therefore recommended to continue with field trials, where the surfactant is directly injected into the flowline.
- Similar experiments can be conducted to find the effect of surfactant on other slug types in the flowline, such as hydrodynamic slugs and terrain slugs. In order to identify relatively short slugs such as hydrodynamic slugs with DAS, a DAS box with a small resolution (i.e. < 1 m) must be selected.

Appendix A

SSL operating guide

1. Fill up both water tanks
   (a) Open HVs to first tank
   (b) Start pump
   (c) Close HVs to the tank and open HVs to second tank
   (d) Open HV 111 at tank to couple both water tanks
   (e) Open HV 122 at other tank to couple both water tanks
2. Fill up separator
   (a) Open butterfly valve at first floor
   (b) Turn on pump P 140 and KCV 140 (labview)
   (c) Water should increase in V 202 (labview) up to about 80%
   (d) Close butterfly valve again at first floor
3. Air/Water injection
   (a) Open air HV 107 at airflow controller
   (b) Open HV 127 and HV 149 at injection point
4. Section 3 (labview)
   (a) Open FCV 352, FCV 351 and FCV 350 to 100%
5. Main (labview)
   (a) Open yellow solenoid valves KCV 105, KCV 106 and KCV 108 next to the V 105 (labview)
   (b) Open FIC 110 at 10 Nm^3/hr
   (c) Open FCV 300sp at 20%
   (d) Turn on HBS 145
6. Closing
   (a) Close FICs and HBS 145 (labview)
   (b) Wait for 0 Nm^3/hr
   (c) Close KCV 105, KCV 106 and KCV 108 (labview)
   (d) Close FCV 300sp
   (e) Wait for Riser PI 309 to be below 1.5 bar
   (f) Close FCV 352, FCV 351 and FCV 350 (Section 3 - labview)
   (g) Close HV 107, HV 127 and HV 149

Appendix B

Additional photos of experimental setup

Figure B.1: The separator (V-202).

Figure B.2: The vessel above the separator (V-201).

Figure B.3: The inspection glass on the horizontal flowline.

Figure B.4: The water vessel (V-140) where the surfactant was added and mixed with the water.

Figure B.5: The Go Pro HERO camera for flow visualization in the riser.

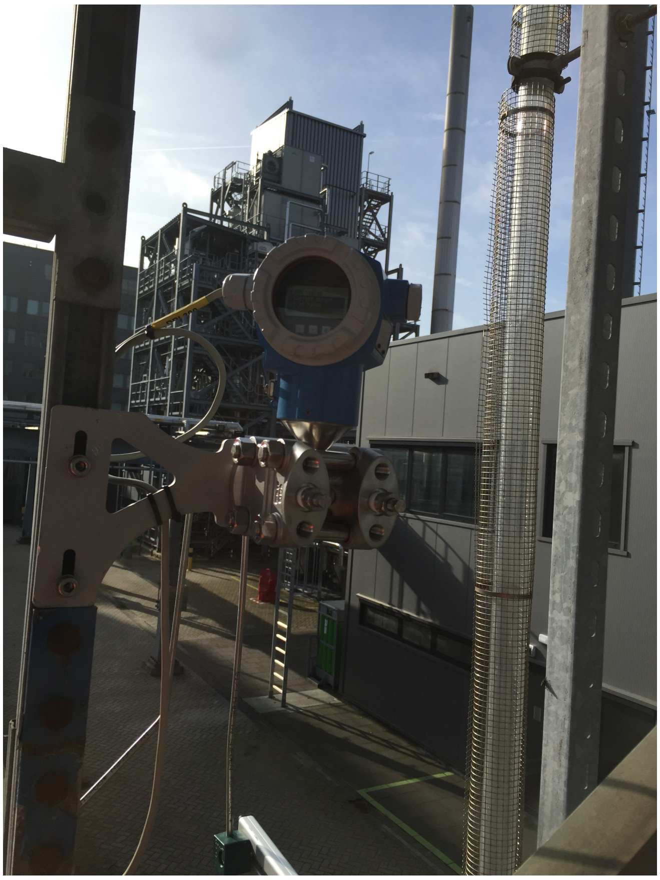

Figure B.6: One of the Pressure Indicators.

Figure B.7: The quick closing valve installed on the riser (KCV-300).

Figure B.8: Photo of the SSL with the vertical riser (installation platform on the left) and the horizontal flowline (all the way to the right).

Figure B.9: Front view of the riser base. Only the middle riser (ID = 44 mm) has been used.

Figure B.10: Side view of the riser base, also showing the injection points of both water and air.

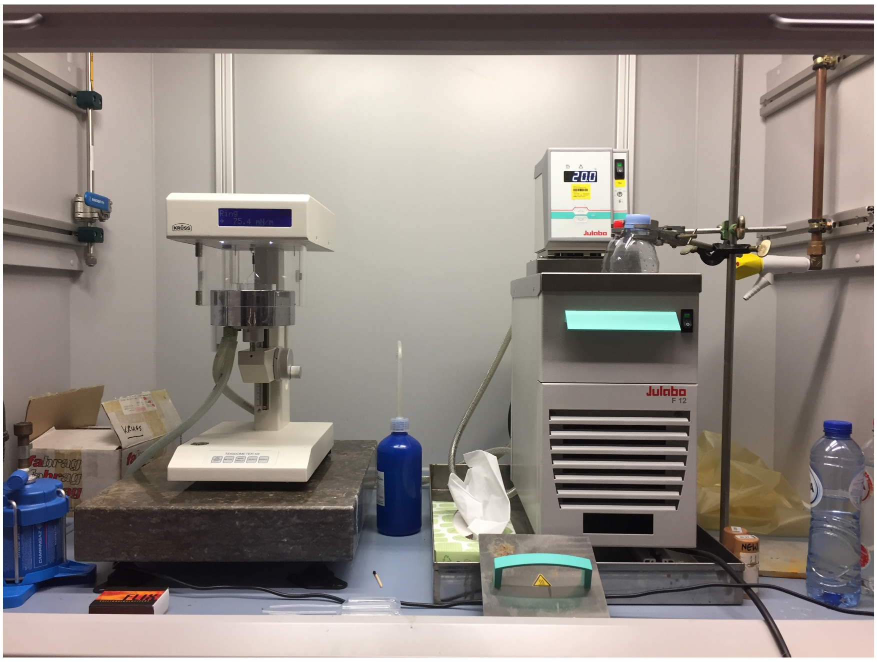

Figure B.11: The surface tensionmeter in the lab of STCA

Figure B.12: Foam which is vented to the atmosphere with the air from the separator.

Appendix C

Technical drawing Severe Slugging Loop

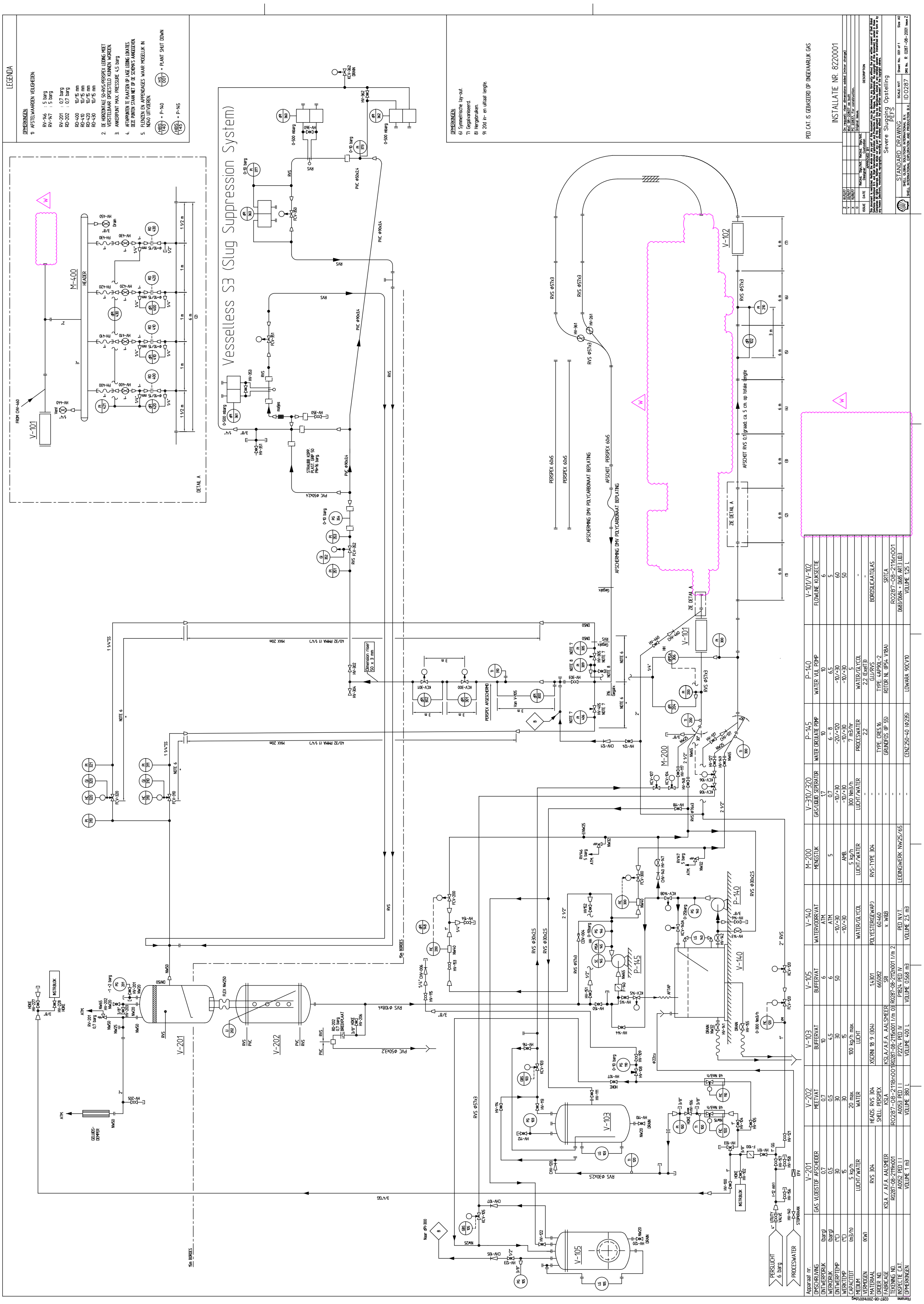

Figure C.1: Technical drawing of the Severe Slugging Loop as in the first configuration located at the outside plot at STCA.

Appendix D

Safety with respect to operating the Severe Slugging Loop

As an operator of the SSL, one has to follow safety requirements:

- Before entering the outdoor plot at STCA, one has to complete an outdoor training. During this training, general safety issues are discussed. This includes the discussion of the emergency exits, the actions to be taken while in emergency and the required protection gear
- At the outdoor plot, one is required to wear Protective Personal Equipment (PPE), consisting of a helmet, protection glasses, safety shoes and a lab or orange operator jacket
- The operator controls the SSL in the porto cabin next to the SSL, which provides extra protection

Furthermore, the SSL was designed in such way, that it includes the following safety checks:

- The maximum operational pressure is 6 bara. This is the maximum pressure that the perspex segments in the flowline and riser can allow. In case this pressure is exceeded, a relieve valve will open, releasing water and air to the ambient. The relieve valve is located downstream of the STCA air supply, and upstream of the air entering the flowline
- The SSL has a "fail safe" design. In case of a power failure, the loop will be shut down automatically. This includes shutting down the water pumps, the flow controllers and the closing of the pneumatic actuated valves
- A RT2 graphite rupture disk is installed downstream of the separator. The disk will rupture and water can be released to the ambient, in case the pressure inside the separator exceeds 0.7 barg ± 10% at 20 °C
- Due to large pressures, weather and light exposure, the perspex pipe segments have failed and have burst some years ago. To prevent injuries to people or damage to the surrounding equipment, the segments are covered by a metal chicken mesh

The incident

In this research, the perspex tubing in the SSL has also failed during operation. At the top of the riser, right before the bend, the tubing did burst. The following occurred. The loop was being operated at Q_{air} = 177 Nm^3/hr and Q_{water} = 1.77 m^3/hr. In order to measure the liquid holdup, the quick closing valves are shut which initiates 2 automatic actions: 1) the water pump shuts off, and 2) the air control valves shut. In this way, the system cannot over pressurize when the quick closing valves are shut. Right after the liquid holdup had been measured, the quick closing valves were re-opened. This is when it went wrong and the perspex piping at the top of the riser did burst. The following Powerpoint slides were used in a meeting in which the incident was reported.

Schematic overview SSL

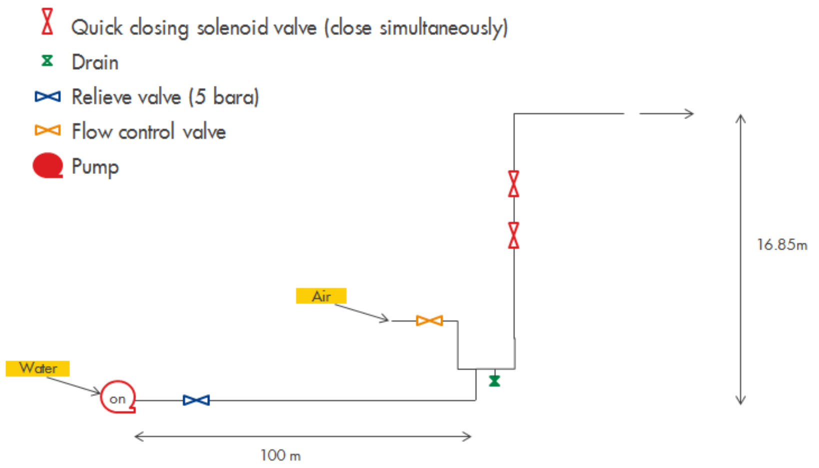

Company name appears here 30 October 2017 2

The use of quick closing valves

When quick closing valves are shut:

- The pump is shut automatically
- The air control valve is shut automatically

So no extra energy inserted in system

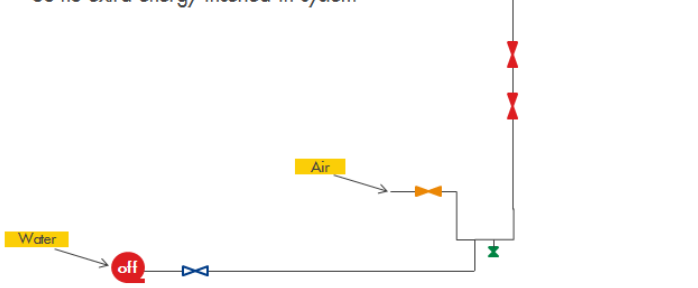

Company name appears here 30 October 2017 3

What happened?

Quick closing valves were opened again

- Water+air hit the bend on top of riser
- Pespex piping burst

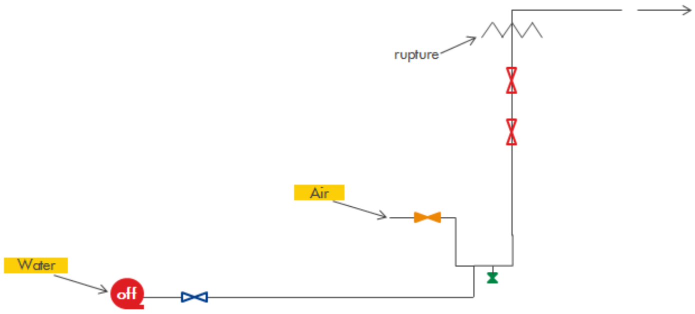

Company name appears here 30 October 2017 4

Pictures of the burst

Company name appears here 30 October 2017 5

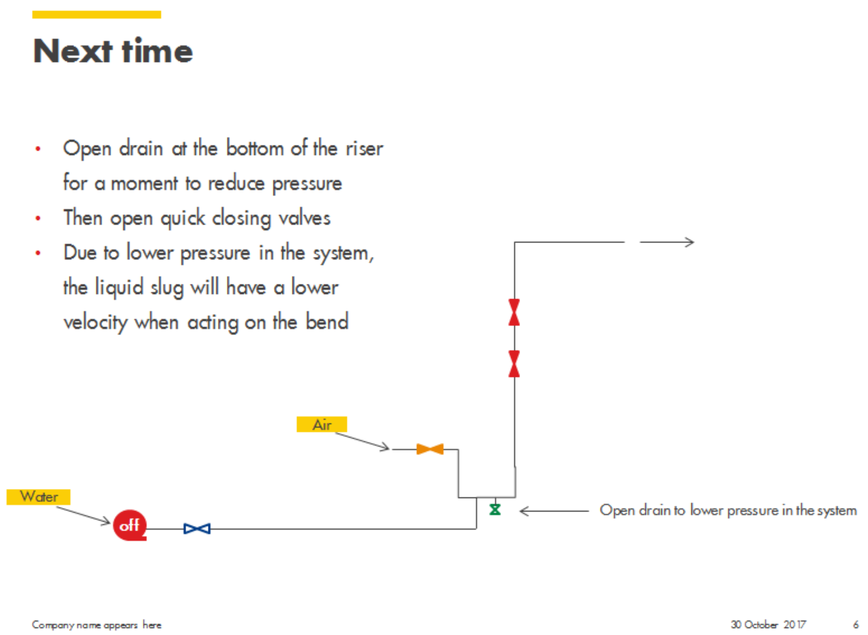
Next time
Open drain at the bottom of the riser for a moment to reduce pressure
Then open quick closing valves
Due to lower pressure in the system, the liquid slug will have a lower velocity when acting on the bend
Air
Water
off
Open drain to lower pressure in the system
Company name appears here
30 October 2017
6

Appendix E

OptaSense DxS Browser

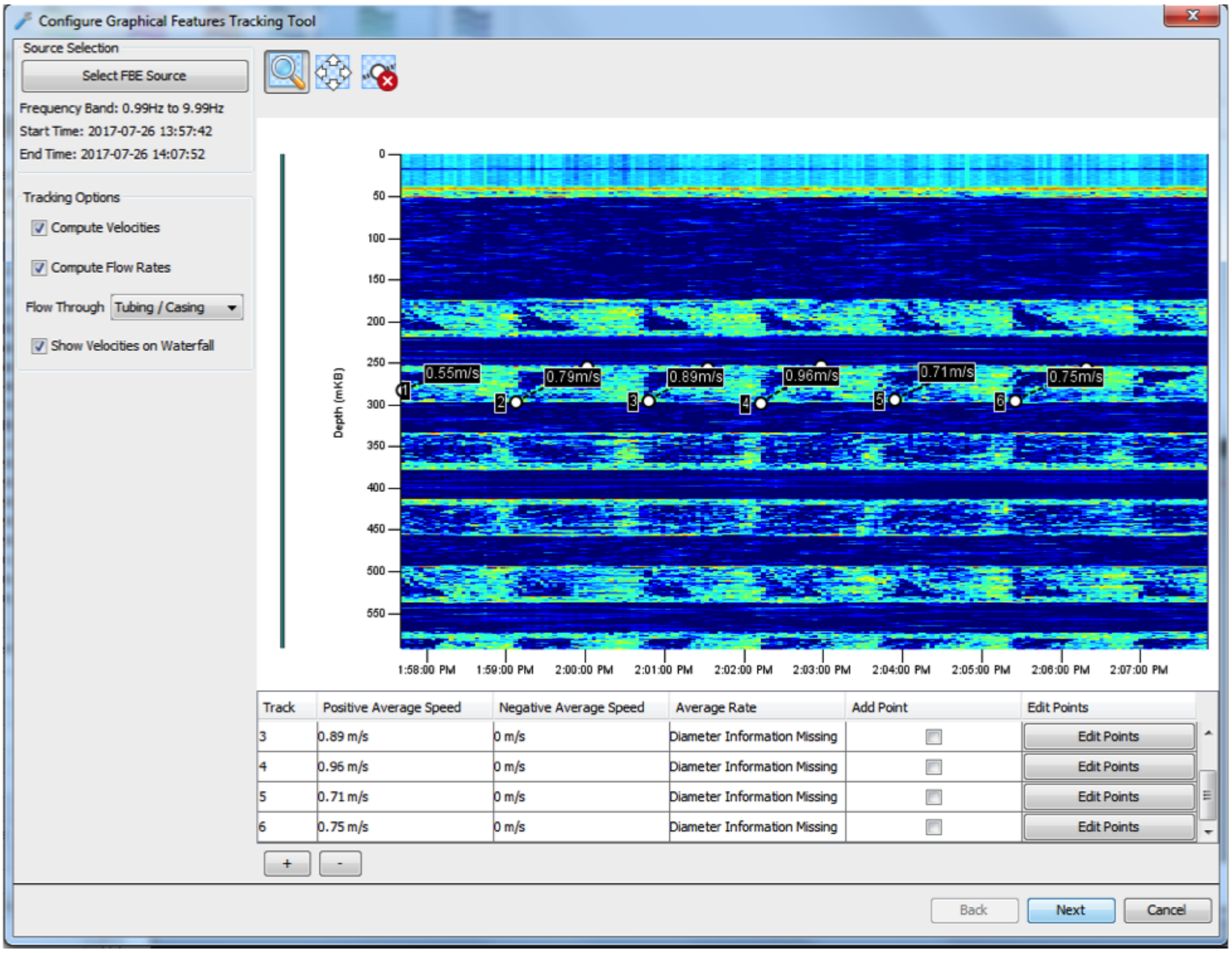

Figure E.1: The velocity tracking tool in the OptaSense DxS Browser software.

Appendix F

Severe slugging

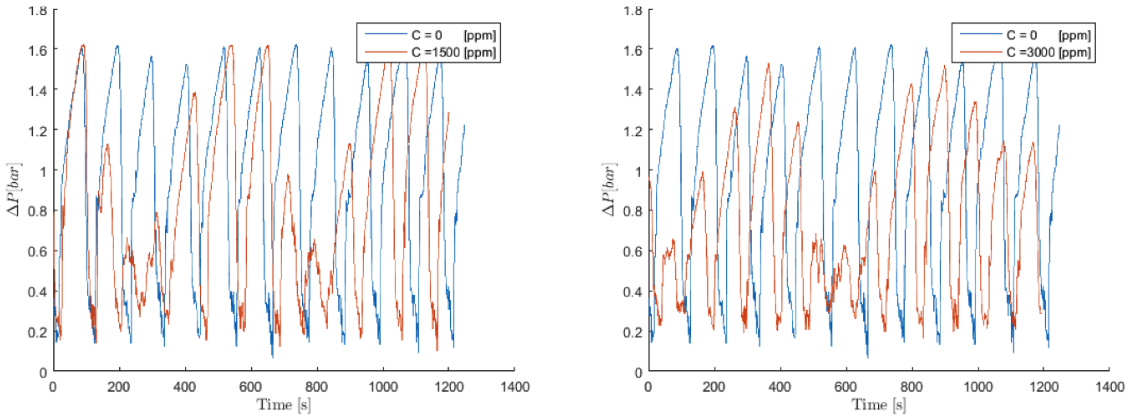

(a) C_{eff} = 1500 ppm

(b) C_{eff} = 3000 ppm

Figure F.1: Riser pressure drop for a severe slugging cycle with u_{sg} = 1.42 m/s and u_{sl} = 0.27 m/s.

Appendix G

Slugging in the riser

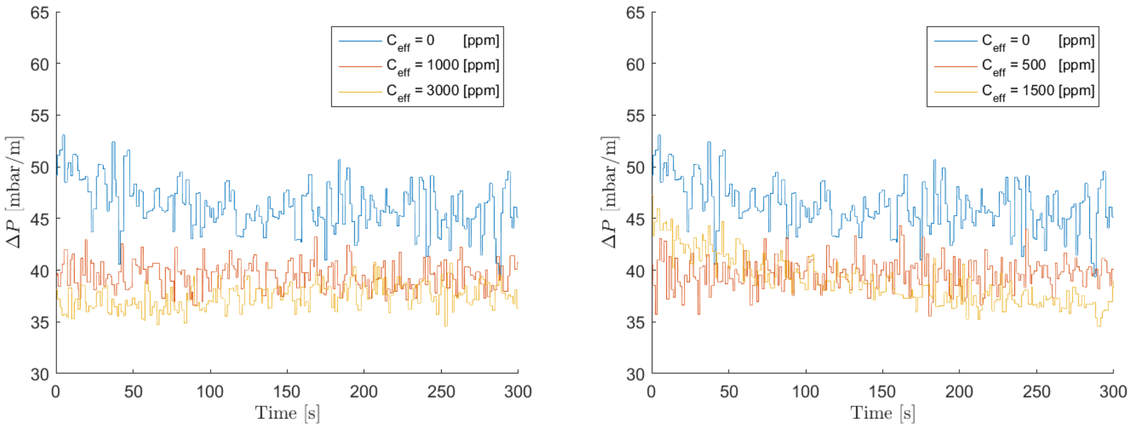

(a) DPI-301 (halfway the riser) (b) DPI-301 (halfway the riser)

Figure G.1: Comparison of differential pressure measured halfway on the riser of the SSL for multiple surfactant concentrations. Measurements were taken at u_{SG} = 0.37 m/s and u_{SL} = 0.27 m/s.

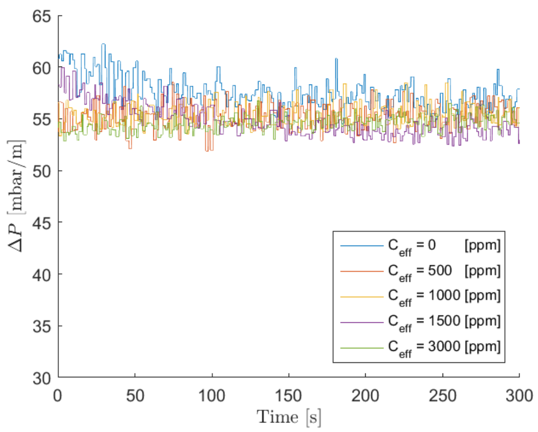

Figure G.2: Comparison of differential pressure measured at the riser base (DPI-300) of the SSL for multiple surfactant concentrations. Measurements were taken at u_{SG} = 0.37 m/s and u_{SL} = 0.27 m/s.

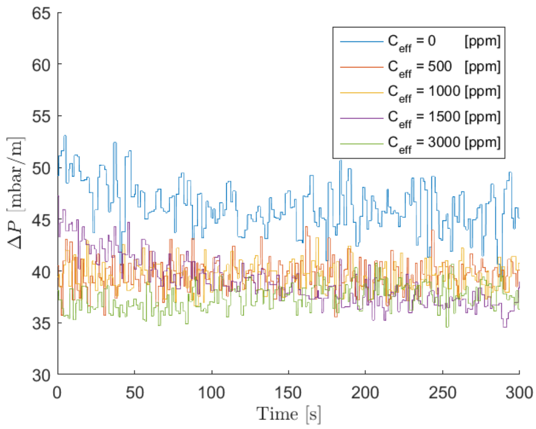

(a) DPI-301 (halfway the riser)

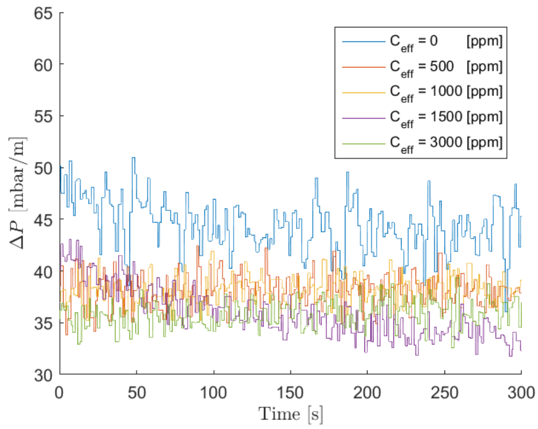

(b) DPI-302 (top of the riser)

Figure G.3: Comparison of differential pressure measured on two locations on the riser of the SSL for multiple surfactant concentrations. Measurements were taken at $u_{SG} = 0.37$ m/s and $u_{SL} = 0.27$ m/s.

Appendix H

Pressure gradient

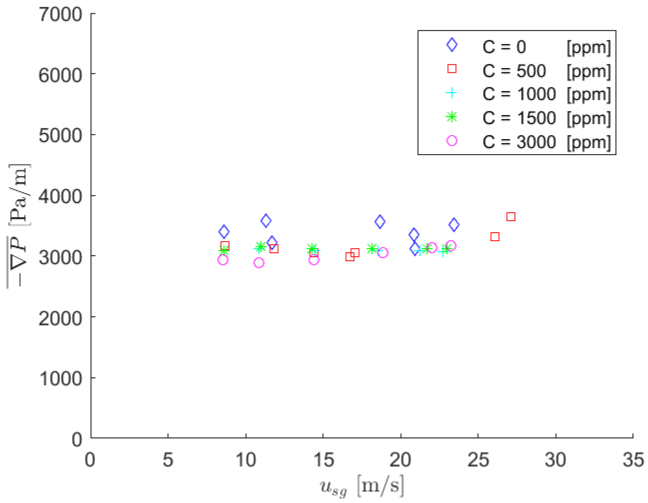

Figure H.1: Comparison of TPCs for different effective concentrations of surfactant in air-water. Measurements were taken with u_{SL} = 21.2 m/s

Appendix I

Pressure gradient findings by Van Nimwegen (2015)

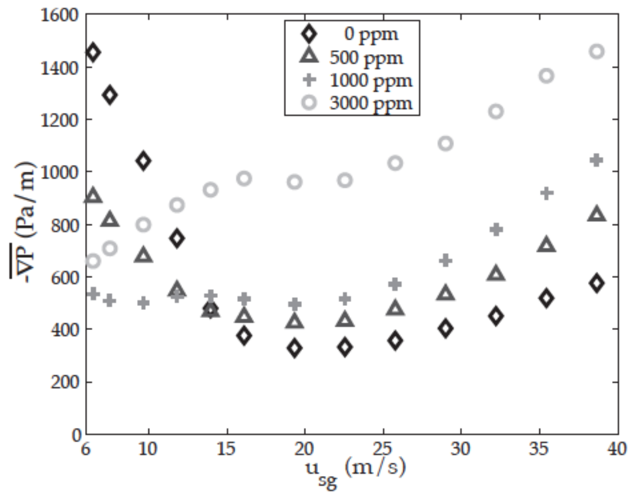

Figure I.1: Comparison of TPCs for different effective concentrations of surfactant. Measurements were taken at constant u_{SL} = 0.01 m/s [1].

Appendix J

Flow development findings by Van Nimwegen (2015)

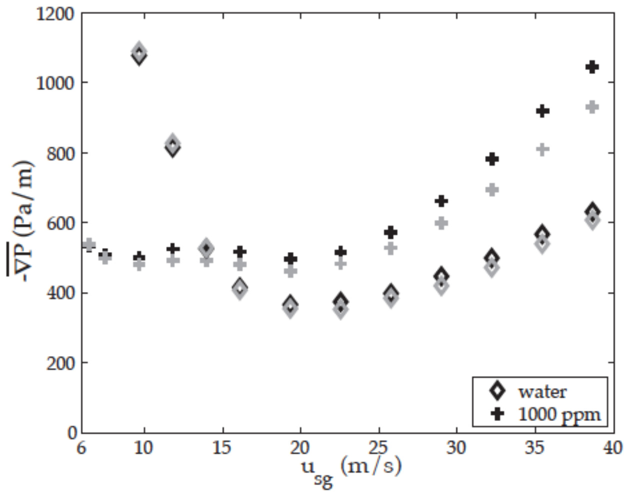

Figure J.1: Comparison of the pressure gradient between 6 m and 8 m (120-160D, grey symbols) and between 8 and 10 m (160-200D, black symbols) from the water injection point; u_{SL} = 10 mm/s, the diameter is 50 mm and the surfactant concentration is 1000 ppm [1].

Appendix K

Liquid and foam holdup findings by Van Nimwegen (2015)

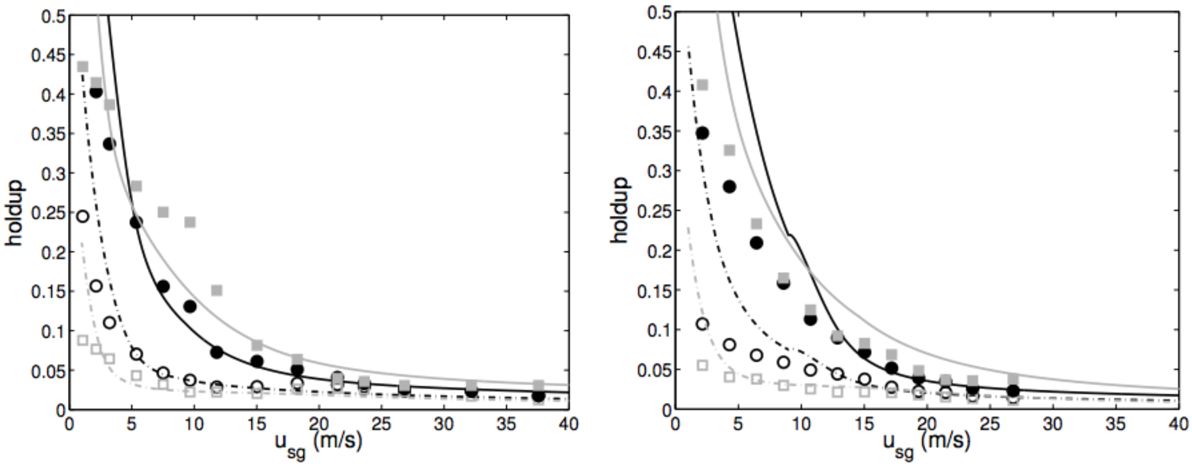

Figure K.1: Holdup fraction with and without foam for the 34 mm setup (left) and the 80 mm setup (right). The lines are the model results, the symbols are the experimental results. Closed symbols and solid lines indicate the holdup fraction of foam and free liquid just after closing the valves. Open symbols and dashed lines indicate the holdup fraction of liquid after the collapse of foam. The circles indicate an effective surfactant concentration of 1000 ppm, the squares indicate an effective concentration of 3000 ppm [4].

Appendix L

Liquid and foam holdup simulation results

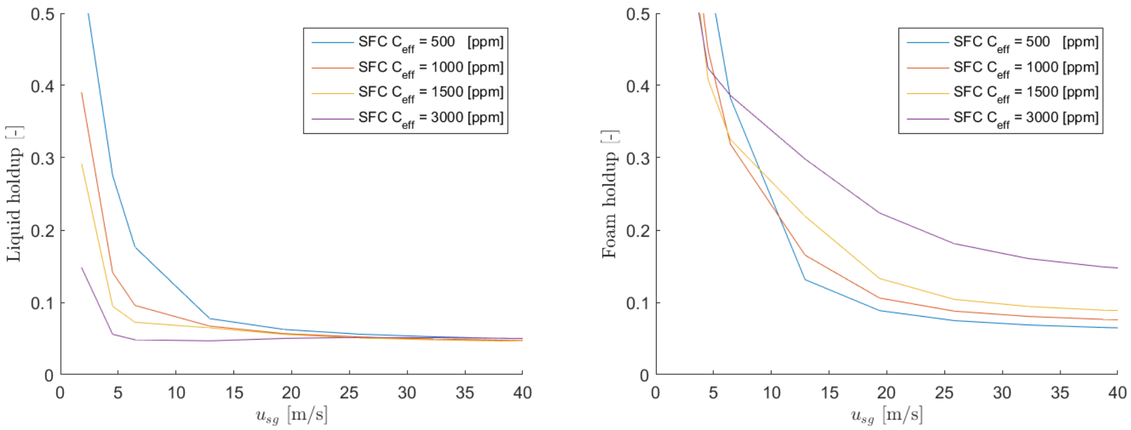

(a) Liquid holdup

(b) Foam holdup

Figure L.1: Comparison liquid and foam holdup simulation results with the Shell Flow Correlations (SFC) for a GLR = 100.

Bibliography

[1] A.T. van Nimwegen. *The Effect of Surfactants on Gas-Liquid Pipe Flows.* PhD thesis, Delft University of Technology, 2015.

[2] A.T. van Nimwegen. The effect of surfactants on flow in gas wells - field analysis and modelling. Technical Report SR.16.10081, Nederlandse Aardolie Maatschappij B.V., 2016.

[3] A.T. van Nimwegen, L.M. Portela, and R.A.W.M. Henkes. The effect of surfactants on upward air-water pipe flow at various inclinations. *International Journal of Multiphase Flow*, 78:132–147, January 2016.

[4] A.T. van Nimwegen, L.M. Portela, and R.A.W.M. Henkes. Modelling of upwards gas-liquid annular and churn flow with surfactants in vertical pipes. *International Journal of Multiphase Flow*, 09 2017.

[5] C.E. Brennen. *Fundamentals of multiphase flow.* Cambridge University Press, 2005.

[6] D. Weaire. The rheology of foam. *Colloid & Interface Science*, 13:171–176, 2008.

[7] G.-D. Xia, and L. Chai. Influence of surfactant on two-phase flow regime and pressure drop in upward inclined pipes. *Journal of Hydrodynamics*, 24:39–49, 2012.

[8] J.F. Lea, H.V. Nickens, and M.R. Wells. *Gas Well Deliquification.* Elsevier Inc., 2008.

[9] J.M.C. van 't Westende. *Droplets in annular-dispersed gas-liquid pipe-flows.* PhD thesis, Delft University of Technology, January 2008.

[10] M. Kerem. RTD-4 Foam Assisted Gas Lift Trial - Field Data and Well Performance Analysis. Technical Report SR.16.13356, Shell Global Solutions, 2016.

[11] L. Liu, X. Li, L. Tong, and Y. Liu. Effect of surfactant additive on vertical two-phase flow. *Journal of Petroleum Science and Engineering*, 115:1–10, March 2014.

[12] P.-G. de Gennes, F. Brochard-Wyart, and D. Quere. *Capillarity and Wetting Phenomena: Drops, Bubbles, Pearls, Waves.* Springer, 2004.

[13] P. in 't Panhuis. Distributed Acoustic Sensing - A Primer on the Application of DAS for Downhole Flow Monitoring. Technical Report SR.15.11964, Shell Global Solutions, August 2015.

[14] P. in 't Panhuis, R. Kusters, L. Groen. Second das field trial for flow assurance in brunei. Technical Report SR.12.10291, Shell Global Solutions, January 2012.

[15] R. Malekzadeh. *Severe slugging in gas-liquid two-phase pipe flow.* PhD thesis, Delft University of Technology, 2012.

[16] R.A.W.M. Henkes. Guidelines for the hydraulic design and operation of multiphase flow pipeline systems. Technical Report SR.14.12950, Shell Global Solutions, May 2015.

[17] R.A.W.M. Henkes. Ormen Lange Low FLow Production - Feasability of using a foamer for pipeline deliquification. Shell Projects & Technology, 2016.

[18] R.H.A. IJzermans, R. Lacy. Technical description Shell Flow Correlations. Technical Report GS.09.51663, Shell Global Solutions, May 2009.

[19] R.I. Christiansen. A new look at foam for unloading gas wells. Technical Report Technical Report 2774, Colorado School of Mines, Golden, USA, 2006.

[20] R.J. Pugh. Foaming, foam films, antifoaming and defoaming. *Advances in Colloid and Interface Science*, 64:67–142, February 1996.

[21] R.V.A. Oliemans. Applied multiphase flows, November 1998.

[22] S.A. Hosseini, A.A. Jalali Khalilian. Considerations in designing multiphase flow lines. *Pipeline & Gas Journal*, 239(8), August 2012.

[23] T. Duangprasert, A. Sirivat, K. Siemanond, and J. O. Wilkes. Vertical two-phase flow regimes and pressure gradient under the influence of sds surfactant. *Experimental Thermal and Fluid Science*, (32):808–817, 2008.

[24] Y. Taitel. Flow pattern transition in rough pipes. *International Journal of Multiphase Flow*, 3:597–601, June 1977.